



8-2010

# System Development And Integration Of An Airborne Laser Communications Payload For Unmanned Aircraft Systems

Mariusz Czarnomski

Follow this and additional works at: <https://commons.und.edu/theses>

 Part of the [Electrical and Computer Engineering Commons](#)

## Recommended Citation

Czarnomski, Mariusz, "System Development And Integration Of An Airborne Laser Communications Payload For Unmanned Aircraft Systems" (2010). *Theses and Dissertations*. 2528.

<https://commons.und.edu/theses/2528>

This Thesis is brought to you for free and open access by the Theses, Dissertations, and Senior Projects at UND Scholarly Commons. It has been accepted for inclusion in Theses and Dissertations by an authorized administrator of UND Scholarly Commons. For more information, please contact [zeinebyousif@library.und.edu](mailto:zeinebyousif@library.und.edu).

SYSTEM DEVELOPMENT AND INTEGRATION OF AN AIRBORNE LASER  
COMMUNICATIONS PAYLOAD  
FOR UNMANNED AIRCRAFT SYSTEMS

by

Mariusz Czarnomski

Bachelor of Science, University of North Dakota, 2010

A Thesis

Submitted to the Graduate Faculty

of the

University of North Dakota

in partial fulfillment of the requirements

for the degree of

Master of Science


Grand Forks, North Dakota

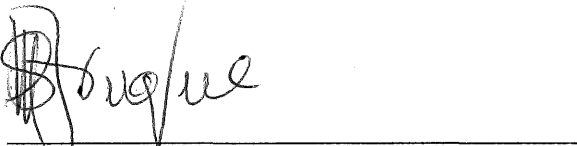
August

2010

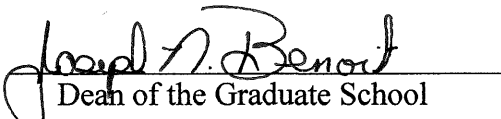
This thesis, submitted by Mariusz Czarnomski in partial fulfillment of the requirements for the Degree of Master of Science from the University of North Dakota, has been read by the Faculty Advisory Committee under whom the work has been done and is hereby approved.

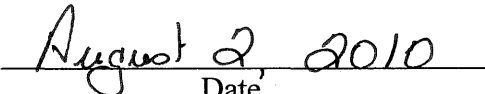
  
\_\_\_\_\_  
(Chairperson)

  
\_\_\_\_\_

  
\_\_\_\_\_

This thesis meets the standards for appearance, conforms to the style and format requirements of the Graduate School of the University of North Dakota, and is hereby approved.

  
\_\_\_\_\_  
Dean of the Graduate School

  
\_\_\_\_\_  
Date

PERMISSION

Title            System Development and Integration of an Airborne Laser  
                      Communications Payload for Unmanned Aircraft Systems

Department    Electrical Engineering

Degree         Master of Science

In presenting this thesis in partial fulfillment of the requirements for a graduate degree from the University of North Dakota, I agree that the library of this University shall make it freely available for inspection. I further agree that permission for extensive copying for scholarly purposes may be granted by the professor who supervised my thesis work or, in his absence, by the chairperson of the department or the Dean of the Graduate School. It is understood that any copying or publication or other use of this thesis or part thereof for financial gain shall not be allowed without my written permission. It is also understood that due recognition shall be given to me and to the University of North Dakota in any scholarly use which may be made of any material in my thesis.

Signature

A handwritten signature in cursive script, appearing to read "D. M. L.", written over a horizontal line.

Date

8/25/2010



## TABLE OF CONTENTS

LIST OF FIGURES .....	VII
LIST OF TABLES .....	X
ACKNOWLEDGMENTS .....	XI
ABSTRACT .....	XIII
CHAPTER	
1.    INTRODUCTION .....	1
Project Overview .....	1
System Requirements.....	4
Subsystems.....	5
UAS Platform.....	6
Literature Review.....	7
Thesis Organization .....	11
2.    LASER COMMUNICATIONS SUBSYSTEM .....	13
Laser Transmitter (TX).....	13
Laser Receiver (RX) .....	16
3.    TWO-AXIS GIMBAL POINTING SUBSYSTEM.....	22
Flight Computer .....	22
Gimbal Control System.....	29
Mechanical Mounting .....	30

	Automatic Tracking Algorithm.....	32
	Coordinate System Definition.....	33
	Kinematic Analysis of the System.....	33
	Software Implementation.....	36
	Joystick Control .....	38
4.	STEPS IN THE INTEGRATION PROCESS.....	42
	Crucial System Components.....	42
	Airborne Components.....	42
	Ground-Based Components .....	48
	UAS Platform.....	49
	Autopilot Integration.....	50
	Steps in the Process of Integration.....	50
	Hardware Integration .....	55
5.	TESTING.....	58
	Preliminary Component Tests.....	58
	Laser Transmitter .....	58
	Laser Receiver .....	60
	Bandpass Filter.....	61
	On-board Computer .....	62
	Position Sensing Diode (PSD).....	63
	Joystick Software Test .....	66
	Gimbal Optimization .....	67
	System Tests .....	68

	Simulations .....	70
	Flight Tests.....	71
6.	SUMMARY AND FUTURE RECOMMENDATIONS .....	76
	Machine Vision-based Tracking .....	76
	Laser Modulation .....	77
	Receiver Improvements .....	77
	Gimbal Improvements .....	78
	Software Refinement .....	79
	Conclusion .....	80
	APPENDIX A: Wiring Diagram of PC 104+ Components.....	81
	APPENDIX B: MSMX104+ Serial Port Pin Out .....	82
	APPENDIX C: LAN 1 and LAN 2 Internet Connectors Pin Out.....	83
	APPENDIX D: Ground-based Computer MATLAB Code for Joystick Control.....	84
	APPENDIX E: On-board Computer Split MATAALB Code for Joystick Control.....	89
	APPENDIX F: The Super Hauler Model as it Appears in .txt File Read by Autopilot.....	91
	APPENDIX G: Controller gains settings in Piccolo Command Center .....	95
	REFERENCES .....	100

## LIST OF FIGURES

Figure	Page
1 Gimbal system with laser head and electro-optical (EO) camera attached (left), and the laser photodiode array receiver (right).....	3
2 Laser beam expander .....	3
3 PSD rear and front view. The photodiode area is $1 \times 1 \text{ cm}^2$ .....	3
4 System block diagram.....	6
5 Solar energy density over different wavelengths.....	14
6 Responsivity curve of the photodiode used in the RX photodiode array. Image courtesy <a href="http://silicon-sensor.com">http://silicon-sensor.com</a> .....	16
7 Original laser receiver with the receiving photodiode in front.....	16
8 Laser RX diagram design in Electronics Workbench.....	18
9 Laser RX circuit built on a breadboard with an array of six photodiodes.....	18
10 The PCB prototype of the laser RX.....	19
11 Laser RX box.....	20
12 Bandpass filter specification.....	21
13 PC 104+ computer and its enclosure. ....	23
14 Versa Teiner end plates and fan placement. ....	24
15 PC 104+ power input wiring diagram. ....	24
16 Computer stack before adding the serial port expansion board.....	25
17 Computer stack after adding the serial port expansion board.....	26

18	Custom built cable for four serial ports.....	27
19	Two-axis pan-tilt gimbal system and motor controller.....	29
20	CAD representation of the mechanical mounting apparatus, the two-axis gimbal, laser transmitter, and EO camera.....	31
21	Orientation of inertial coordinates.....	33
22	Simulink block diagram for Embedded MATLAB.....	37
23	Joystick used to manually control the gimbal and SONY camera. Courtesy: <a href="http://ecx.images-amazon.com/images/I/414X2Z0A7TL._SL500_AA280_.jpg">http://ecx.images-amazon.com/images/I/414X2Z0A7TL._SL500_AA280_.jpg</a> .....	38
24	Snapshot of the MATLAB pop up window with the joystick buttons function assignment.....	39
25	Three functions available for the joystick velocity control of the gimbal.....	40
26	Laser TX board with aluminum laser diode head enclosure and extension wires.....	43
27	ELVIS payload mount inside of the Super Hauler payload bay.....	45
28	Assembly of gimbal mount and gimbal system.....	46
29	Mounting configuration of the PC 104+ onboard computer.....	47
30	Super Hauler UAS and its payload bay.....	50
31	UAS autopilot system components. Courtesy: <a href="http://www.cloudcaptech.com">www.cloudcaptech.com</a> .....	51
32	Screenshot from the AVL program.....	54
33	Copper plate shielding and antenna ground plates.....	56
34	Servo harness and ignition wire shielding.....	56
35	Payload bay and aluminum firewall with EMI shielded pass-through hole.....	57
36	Laser TX board with R11 and Q1 annotated.....	60
37	PSD scaling circuit.....	64
38	PSD testing.....	65

39 Aircraft truck mount. ....69

40 Truck test setup.....69

41 Simulation results for a square flight plan.....71

42 Snapshot from the RF video feed during the first flight test, July 28-30, 2009. ....72

## LIST OF TABLES

Table	Page
1 Summary of DGPS and IMU data.....	36
2 Laser diode test.....	59
3 Pass-fail results for serial communications.....	62
4 PSD tests and associated pass-fail criteria.....	63
5 Pass-fail results table for joystick software.....	66
6 Gimbal optimization test table (split in half).....	67

## ACKNOWLEDGMENTS

First of all, I would like to thank my academic advisor, Dr. Richard R. Schultz, for making this accomplishment possible for me. Without his help in designing my curriculum and constantly helping me with my class selection, I would not be able to graduate with my bachelors and masters degrees in three-and-a-half years. Furthermore, I would like to thank him for being an outstanding mentor, and source of great advice, not only in the work place or classroom, but also in all those little things pertaining to everyday life. His wisdom and words of encouragement in times when morale was low helped me to see the light at the end of the tunnel and made me believe in myself.

I would also like to thank Dr. William H. Semke for his always critical words of advice, advice that acted as a wakeup call and kept me focused, down to the ground, and on the task, even if it meant to delay the project by a few weeks. His expertise and professionalism made me think outside the box and taught me to pay attention to details.

This achievement would not be possible without all the knowledge that I gained from the helpful faculty in the Department of Electrical Engineering, who are always open to suggestions. I do believe that countless hours of lectures and endless nights spent on assignments and projects gave me the necessary background to confidently and successfully step into the job market, and deliver the highest quality engineering services.



In addition to faculty and advisors, I would like to thank one of my peers and work partner, Jason Blakely. His bright ideas and need for constant improvement helped me to bring this project to the next level, and made me realize that there are answers to all the questions, one just needs to keep looking for them.

This accomplishment would be possible without the help of all members of the Unmanned Aircraft System Engineering Laboratory, which receives its financial assistance from the Department of Defense contract number FA4861-06-C-C006, “Unmanned Aerial System Remote Sense and Avoid System and Advanced Payload Analysis and Investigation,” and the North Dakota Department of Commerce, “UND Center of Excellence for UAV and Simulation Applications.”

Last but certainly not least, I would like to express my warmest words of appreciation to my dearest wife, Tiffany, for all the words of encouragement she offered me throughout all the years spent in school. Sometimes just her presence was enough to give me a boost of energy to keep me going forward. Being able to see her commitment and perseverance in pursuit of her own degree made me want to be a better student, a better husband, and a better man.

## ABSTRACT

Free space laser communications provides wide bandwidth and high security capabilities to Unmanned Aircraft Systems (UAS) in order to successfully accomplish Intelligence, Surveillance, Target Acquisition, and Reconnaissance (ISTAR) missions. A practical implementation of a laser-based video communications payload flown by a small UAS aircraft is described as a proof-of-concept. The two-axis gimbal pointing control algorithm calculates the line-of-sight vector in real-time by using Differential Global Positioning System (DGPS) and Inertial Measurement Unit (IMU) information gathered from the UAS vehicle's autopilot so that the laser transmitter in the airborne payload can accurately track a ground-based photodiode array receiver with a known DGPS location. One of the future goals of this project is to move from UAS-to-ground communications to UAS-to-UAS free space laser communications.

A communications system has been developed using Light Amplification by Stimulated Emission of Radiation (LASER) to transmit data to a known location on the ground. Several main subsystems including the laser transmitter, laser receiver, gimbal, subsystem, and tracking software are discussed, along with the integration and testing phase. The laser transmitter is mounted within the Super Hauler small UAS payload bay. The UAS was custom made in compliance with the Super Hauler requirements, specifically regarding the size and shape of the payload bay. A two-axis gimbal system is controlled via the tracking software to point the laser beam to a specified

DGPS coordinate throughout the flight. In addition to the GPS system, there is a machine vision-based tracking system in development that works in parallel with the GPS system and takes over gimbal control for precise alignment.

At the known DGPS coordinate, the ground-based receiver is stationary and converts the video data carried by the laser to a viewable format. The receiver, like any other subsystem, is a very crucial component of a successful data transmission system; therefore, significant time and effort was designated for its development.

To ensure successful operation of the free space laser communications payload, a series of subsystem tests were performed. For each subsystem, a test procedure was developed with specific pass-fail criteria. After each subsystem was tested, a full system test was also carried out. The full system included the integration of all subsystems inside the payload bay of the Super Hauler UAS. Detailed analyses of the testing procedures along with the integration process are presented in this thesis. After the full system was successfully tested in the laboratory, preliminary flight tests took place in July and October of 2009 within military-restricted airspace over Camp Grafton South, a National Guard training facility in North Dakota, followed by another flight tests in June 2010. While these preliminary flights did not result in video transmission, they were very successful in gathering preliminary data and field test information. These results are crucial in the continued development of the system. Recommendations for future payload improvements are discussed in the last section of this thesis.

## CHAPTER 1

### INTRODUCTION

This chapter serves as an introduction to free space laser communications, and presents the incentive behind designing and building the Enhanced Laser Video Integrated System, henceforth referred to as the ELVIS payload. It also presents the background of the ELVIS project and an outline of its current implementation. The organization of this thesis and a review of the relevant literature review is also included at the end of this chapter.

#### 1.1 Project overview

Communications by means of Light Amplification by Stimulated Emission of Radiation (LASER) has been on the scientists' agenda since shortly after the actual invention of the laser in 1960. Military officials were particularly interested in this new, evolving, and exciting technology. The natural advantage of laser communications over traditional radio frequency (RF) communication systems is its narrower beam-width transmission, which concentrates a larger fraction of the transmit power onto the receiver. One of the incentives behind building free space laser communication systems is to improve the security of the current RF based communication systems available on the market. Current communication systems that rely on RF technology to transmit and receive signals are very susceptible to electronic interference, jamming, and interception.

Consequently, in applications where signal reliability and security are paramount, RF communications is not always desirable. The proposed laser system occupies a portion of the frequency spectrum which does not require frequency allocation or clearance from the Federal Communications Commission (FCC). An added benefit of the current method is that the spectrum used for communications is not widely occupied and this gives the system a much larger bandwidth, which in turn allows for more analog and digital data to be transmitted. The point-to-point nature of the laser notably improves the reliability and security of the communications system and significantly lowers the possibility of electronic jamming and interception. The first iteration of this system aims at transmitting a video signal from a UAS vehicle down to the ground via laser link. However, the end goal of this project is to design a laser communications system that will serve as a communications link between two or more airborne UAS platforms. The ELVIS payload consists of an airborne laser transmitter attached to a two-axis gimbal pointing system and a ground-based photodiode array receiver. The gimbal system and the receiver are shown in Figure 1. Additionally, there is an electro-optical (EO) camera with near infrared (IR) filter that can be turned on or off during operation, the laser beam expander shown in Figure 2, and the Position Sensing Diode (PSD) unit for future consideration shown in Figure 3. The purpose of the components is to (a) accurately steer the gimbal to point the laser beam at the transmitter and overcome turbulence associated with aircraft vibration; (b) monitor the performance of the tracking algorithm with the EO camera mounted on the gimbal; (c) utilize the PSD's light detection capabilities for machine vision-based precision tracking; (d) successfully receive the laser beam on the

ground and filter out noise by using bandpass filters; and (e) adjust the size of the laser beam on the ground.

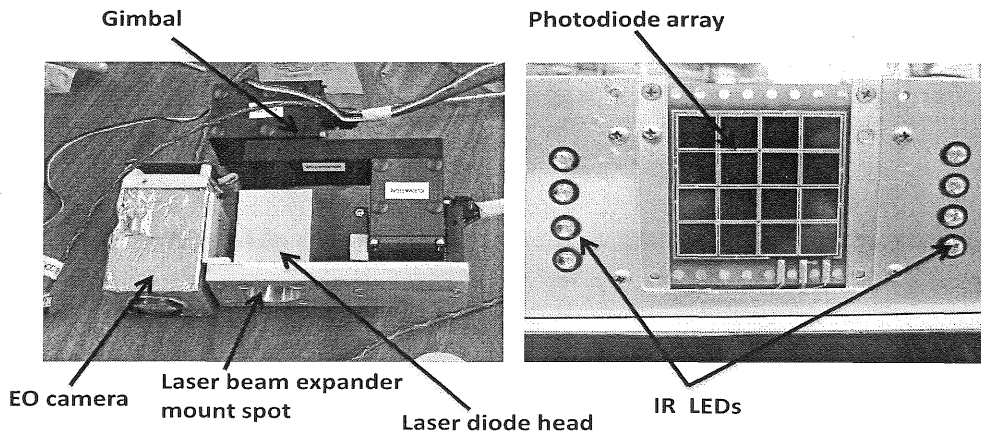
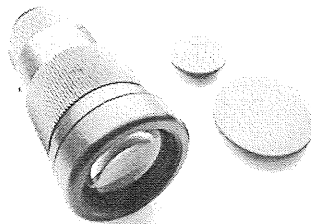
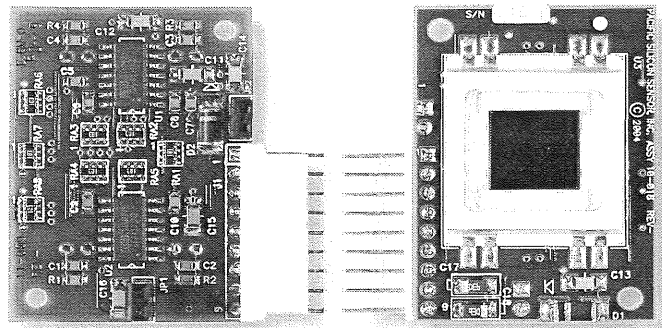


Figure 1: Gimbal system with laser head and electro-optical (EO) camera attached (left), and the laser photodiode array receiver (right).



Courtesy: [dragonlasers.com](http://dragonlasers.com)

Figure 2: Laser beam expander.



Courtesy: <http://www.pacific-sensor.com>

Figure 3: PSD rear and front view. The photodiode area is  $1 \times 1 \text{ cm}^2$ .

## 1.2 System requirements

The UAS free space laser communications system has specific requirements that must to be met in order to complete the communications link. The first requirement is that the UAS maintains a visual line of sight with the ground station receiver. This means that the laser beam must traverse a straight-line path to the receiver without any object compromising this path. Any time that a physical object blocks the laser beam from reaching the receiver, there is a loss of signal and the communications link is broken. Another requirement specific to the laser receiver is that it must withstand any other signal interference caused by ambient light. Reducing the acquisition errors of the pointing algorithm with respect to the UAS's DGPS laser transmitter location and the DGPS specified ground-based receiver location is another requirement that the system must overcome. This means that as the UAS travels in its flight path, atmospheric turbulence causes it to have unwanted movement. In turn, this motion causes the transmitter gimbal pointing system to have additional pointing errors in establishing the communications link with the receiver. The system needs to maintain the aforementioned visual line of sight for as long as possible; however, current UAS flight restrictions limit the range of transmission to a one-half mile radius from the ground station and an altitude of no higher than 3000 feet. Finally, in its current configuration in the Super Hauler UAV built for the UND Unmanned Aircraft Systems Engineering (UASE) laboratory requires that the system's payload be no heavier than 25 pounds, must fit in the payload bay of the aircraft with dimensions of 21" x 11" x 12" (LxWxH), and have a communications range of at least 1000 feet.

### 1.3 Subsystems

Two primary subsystems have been developed. The first consists of a laser communications subsystem, containing a laser transmitter installed in the airborne payload and a photodiode array receiver positioned at a pre-determined, fixed location on the ground. The second subsystem consists of a two-axis gimbal used to aim the laser transmitter beam at the ground-based photodiode array receiver. An optical expander is also integrated into the airborne laser transmitter for focusing the laser beam. To account for aircraft vibrations and DGPS error, a 4.5cm × 4.5cm photodiode array was custom-built to receive the video data carried by the laser beam. The control algorithm for the two-axis gimbal pointing subsystem is executed on a PC-104+ format embedded computer onboard the payload to accurately aim the laser transmitter at the ground-based photodiode array receiver. This algorithm calculates a line-of-sight vector in real-time by using the UAS autopilot's DGPS (latitude, longitude, and altitude) location with an accuracy of approximately 2cm, the UAS autopilot's IMU (roll, pitch, and yaw) data, and the known DGPS location of the receiver on the ground. To improve pointing accuracy, machine vision-based enhanced tracking capabilities in the near IR spectral band will be implemented in the form of a position sensing diode (PSD). To verify performance of the tracking system, a SONY block camera with a near IR filter is installed on the gimbal parallel to the laser transmitter. This setup gives visual feedback, where the video feed is sent to the ground station through an RF link. The two subsystems have been successfully tested in the laboratory, and preliminary flight tests took place on July 28-30, 2009, and October 3-4, 2009, as well as on June 2-4, 2010,



within military-restricted airspace over Camp Grafton South, a National Guard training facility in North Dakota. The system diagram is shown in Figure 4.

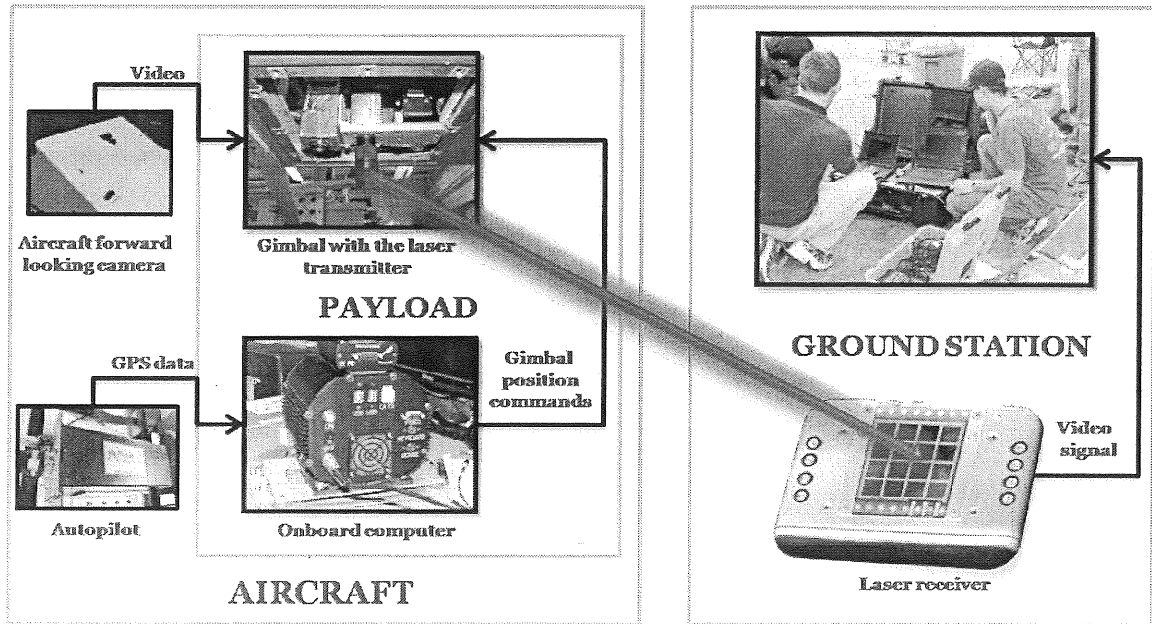


Figure 4: System block diagram.

#### 1.4 Test UAS platform

In order to perform testing of the ELVIS payload and verify its operation, Super Hauler UAS vehicle was used. The aircraft is retrofitted with a Cloud Cap Technology Piccolo II autopilot, and therefore is capable of autonomous flights along with radio-controlled (RC) operations. Due to its extensive user-defined serial ports, the autopilot essentially becomes part of the payload system. Specifically the autopilot RF link is used to communicate with payloads being flown onboard the Super Hauler. A detailed description of the UAS platform is presented in Section 4.2 of this thesis.

## 1.5 Literature review

Due to free space laser communications being a relatively new field, there are not many papers available for review. Additional difficulty in finding relevant sources is the novelty of the ELVIS payload, in which the entire system has been minimized and integrated into a small class UAS. Many of the available papers focus on free space laser communications, where size, weight, and power restrictions are of significantly larger magnitude. Furthermore, most work on laser communications is performed by military or government contractors under classified contracts, and therefore they are not available to the public. In their paper entitled “Space Laser Communications: A Review of Major Programs in the United States [1],” Gerhard A. Koepf et al. present a thorough overview of space laser communications technology and programs developed in the United States between 1960 and 2000. According to Koepf the very first attempt at space-to-ground laser communications along with the first automated tracking of a ground beacon was made in 1965 during the Gemini 7 mission. The link did not get established due to mechanical difficulties surrounding an Argon Ion ground beacon laser. Early attempts proved not only the potential of laser communications, but also the need for extensive development in tracking, acquisition, and transmitter technologies. Throughout the 1960’s and most of the 1970’s, researchers focused on gas lasers, but at the end of the 1970’s, solid state laser technology matured enough to be considered for use in space communications. One of the most popular solid state lasers is the neodymium-doped yttrium aluminium garnet (Nd:YAG) laser. In the mid 1980’s, semiconductor lasers started to gain more popularity due to their improved characteristics in size, efficiency, and potential low cost. One of the first programs that used semiconductor lasers was the

Laser Intersatellite Transmission Experiment (LITE) conducted by MIT Lincoln Laboratory. This paper also talks about deep space laser communications, but that topic is beyond the scope of this thesis.

In the work entitled “Infrared Laser on P3-D,” Karl Meizer et al. [2] present the design of an infrared laser module to be installed on the armature communications satellite called Phase 3-D (P3-D), currently known as AMSAT-OSCAR 40. The work on the laser link started in the summer of 1999, and the satellite was launched in November 2000. This laser downlink is operating at 835nm and delivers data at a rate of about 400bps, with an output power of 500mW. The 400bps bitrate is rather low, but it is enough to transmit telemetry data. An additional restriction is that the data reception can only be performed during the night when ambient light is insignificant. The proposed receiver antenna on the ground has a 10cm diameter and is comprised of avalanche photodiodes. Under those conditions, the laser spot’s diameter on the ground cannot be larger than 1000km, which is extremely large, and the average laser power requirement is 250 mW (500mW with 50% duty cycle). Although 400bps might be enough to transmit telemetry data, it is not sufficient to transmit video data, which requires a data rate of at least 128-384kbs. Since the data rate is directly linked to the sensitivity of the receiver, the 1000km laser spot diameter at 250mW would not be sufficient for video transmission.

Donald Russell et al. [3] present an interesting method for spatial acquisition and fine tracking using one device. In his work entitled “LaserCom Pointing Acquisition and Tracking Control using CCD-based Tracker,” Russell et al. propose to use a single, charged couple device (CCD) camera in a “windowed” read mode to perform both functions. The trick to the design is that a sophisticated custom CCD camera system had

to be developed. The process included the design of both the camera head electronics and processing electronics. The paper was first published in 1994, and the technology has most certainly matured since then, especially with respect to electronics. Therefore, the design presented by Russell does not seem to be as relevant as it was back then, but the concept of using a camera for machine vision based tracking is very promising.

Another interesting paper on acquisition, tracking, and pointing (ATP) of a laser communications system was presented by what seems to be the current leader in public domain laser communications development, the Optical Communication Group at the Jet Propulsion Laboratory (JPL), California Institute of Technology. In the paper entitled "Design and Development of a Robust ATP Subsystem for the Altair UAV-to-Ground Lasercomm 2.5 Gbps Demonstration [4]," G. Ortiz et al. present an elaborate payload design for the mid-size Altair UAS, essentially a Predator-series aircraft, along with the design of the ground receiver station. The Altair platform is capable of lifting 700lbs of internal payload or up to 3000lbs of external payload, has a wing span of 68ft, and is powered by a 700hp propeller engine. The specifications of this UAS allow for much larger and heavier payload designs. The payload system weighs 148lbs and consumes 650W of power. The 2.5Gbps link is necessary for the HDTV images to be transmitted and is achieved by using a 200mW laser at 1550nm. Due to the laser link range of up to 50km, the pointing requirements of the flight terminal are very strict. Ortiz et al. do a very thorough analysis of the link budget in terms of bit error rate (BER), jitter error, and bias error. Their design was based on an existing optical ground station, and also on the Optical Communications Demonstrator (OCD) lasercom flight terminal. The novelty of the system uses an inertial sensor for acquisition and tracking to overcome atmospheric

turbulences, the use of active exposure control to increase the dynamic range to 16dB for beacon tracking, and the implementation of a wide field of view camera for ground beacon acquisition. Another interesting fact is that the laser footprint on the ground needs to be between 1.5m and 3m for a 1m telescope, and the laser beacon footprint on the aircraft needs to be greater than 10m due to the uncertainty of the aircraft location. The onboard receiver has a 10cm aperture terminal. Ortiz et al. use the previously implemented method of a windowed CCD camera for fine tracking, which was also developed at JPL and presented by Russell et al. [5].

A similar project, also from the JPL, was presented by Abhijit Biswas et al. in the paper entitled “Emulating an Optical Planetary Access Link with an Aircraft [6],” In their work, a video signal was sent through a laser communications system from a moving Cessna 206 aircraft down to the ground at distances between 5km and 9km with a data rate of 270Mbs. The enterprise was meant to demonstrate the feasibility of a planetary access link between a ground-based station and a spacecraft orbiting Mars. According to Biswas et al., the novelty of the project lies in the high data rate and volume of data transfer from the ground to the airborne vehicle. Two types of lasers are used: an 808.25nm laser onboard the aircraft for the downlink of a low data rate, pseudo-random bit sequence, and a 1060nm laser for the high data rate uplink. The aircraft illuminates the pre-determined GPS location of the ground-based transceiver with the 808.25nm laser, and the ground transceiver simply awaits the illumination without any knowledge of the aircraft’s GPS location. Once illuminated, the ground transceiver receives the laser signal through a wide field of view camera equipped with a bandpass fish-eye lens centered at 808.25nm. Once illuminated, the ground transceiver starts tracking the

airborne laser using a combination of frame differencing and centroid computation. Next, the 1060nm laser uplink with high data rate is activated, the aircraft transceiver starts closed loop tracking upon receiving the 1060nm laser signal, and sends a low data rate pseudo-random bit sequence to the ground.

Finally, an interesting solution for free space laser communications is presented in the paper entitled “A Combined Laser-Communication and Imager for Micro Spacecraft (ACLAIM) [6],” by H. Hemmati et al. The authors propose a method where the laser communications terminal and the imaging camera share the same telescope. In addition, the ACLAIM has been built using almost exclusively commercial-of-the-shelf (COTS) components. The device is designed to be used onboard very small spacecraft being developed by JPL.

## 1.6 Thesis organization

One of the main components needed for implementing free space optics are the laser transmitter and the laser receiver subsystem. Without this subsystem, free space optics communications does not exist. Chapter 2 presents a detailed overview of the current laser system, the challenges related to free space optical communications, and proposed solutions implemented into the subsystem.

In order to accomplish a successful laser communications link between a moving UAS platform and a stationary ground-based receiver, a precise and stable airborne gimbal pointing system is required. In Chapter 3, the gimbal subsystem is presented. The challenges related to mounting it into the Super Hauler UAS, along with the onboard computer interface, tracking algorithm analysis, and joystick control are discussed.

Chapter 4 of this thesis gathers all the subsystems and walks the reader through the process of integrating them together. This process is not a trivial task, and even though individual subsystems perform well by themselves, they quite often create unforeseen problems when integrated together. This chapter will also talk about difficulties and challenges encountered during the integration process.

No successful project or design exists without extensive testing. For ease of troubleshooting, every subsystem is first tested separately, and then after bringing all the components together and integrating them, the full system test needs to be performed. Sometimes, this is hard to accomplish due to the nature of the project. UAS flight test windows are reserved only a few times a year, and therefore extensive simulation tests in the lab need to take place. Chapter 5 presents detailed testing of the individual subsystems, as well as full system test and simulation. Last but not least, UAS flight tests are discussed at the end of this chapter.

Chapter 6 summarizes the entire project and lists suggestions for future improvements of the ELVIS payload. Recommendations for individual components are presented, along with overall system suggestions.

## CHAPTER 2

### LASER COMMUNICATIONS SUBSYSTEM

The free space laser communications subsystem consists of two main components: the laser transmitter (TX) and the laser receiver (RX). Together, they create a safe and reliable communications system capable of high data rates, as an alternative to the traditional radio-frequency (RF) link which uses an over-allocated region of the electromagnetic spectrum and is susceptible to both electronic jamming and interception. This chapter will serve as a detailed overview of the laser communications subsystem.

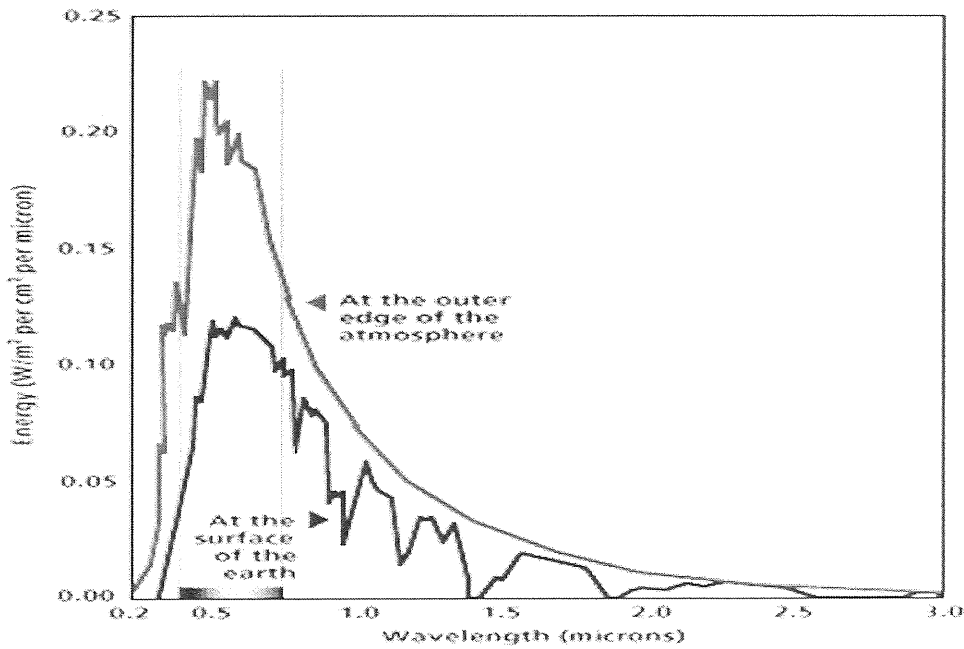
#### 2.1 Laser transmitter (TX)

The current laser transmitter used in the system is a modified version of the IF-VL30 manufactured by Industrial Fiber Optics, a commercial-off-the-shelf (COTS) laser TX unit [7]. This TX was chosen after an extensive trade study based on available budget and size and weight constraints dictated by the dimensions of the Super Hauler's payload bay. The original system came with a 5mW red laser at 640nm. The beam diameter was around 3.2mm, with the maximum beam divergence of 2milliradians. The TX is capable of analog amplitude modulation of 100Hz to 10MHz, and digital amplitude modulation of 0 to 20MHz. According to the device's manual [8], the digital input can be used for a computer-to-printer through-the-air link, a digitally-coded security system, or a



long-distance remote control. The digital input is compatible with standard TTL logic powered by +5volts.

In order to achieve successful communications over longer distances, a 200mW laser diode in the near infrared spectrum at 808nm was installed. There are a few reasons why this particular wavelength was chosen. First of all, the energy coming from the sun that reaches the surface of the Earth varies as a function of wavelength. Figure 5 shows the energy spectrum of the sun. As one can see, right around the 800nm region, there is a significant drop in the amount of energy that gets to the surface of the Earth. This has to do with the ambient light from the sun hitting the RX. If the laser operates at a wavelength where there is less energy interference, there are better chances for successful transmission.



Courtesy <http://energy.saving.nu/solarenergy/sespectrum.gif>

Figure 5: Solar energy density over different wavelengths.

Additionally, the sensitivity of the photodiodes in the receiver is near their peak value at 800nm. Thus, exciting the receiver should be easier with the new laser diode, or consequently we should be able to transmit data over longer distances. The spectral responsivity graph for the receiver photodiode can be found in Figure 6 [9]. The signal that is transmitted over the laser light comes from the onboard, forward-looking visible light camera installed on the Super Hauler and is then amplitude-modulated onto the laser beam. The nature of a standard laser diode at 808nm produces an oval-shaped laser beam, which is not desirable for this particular application due to an irregular and enlarged laser spot on the ground. Originally, in order to correct for that anomaly, an anamorphic prism pair was to be installed at the output of the laser diode. The anamorphic prism pair consists of two prisms aligned to expand a beam in only one direction, circularizing the elliptical output from a diode. However, after visiting with one of the vendors from Blue Sky Research at the 2010 SPIE LASE conference, we were introduced to a laser diode at 808nm that produces a circular beam output with diffraction-limited performance and low divergence in a standard package [10]. These attributes are achieved through the integration of internal, beam correcting optics. The decision was made to purchase that diode and integrate it into our system. To further ensure a more coherent and directed laser beam, a laser beam expander from dragonlasers.com [11] was also installed at the output of the laser diode. Knowing the altitude of the flight path, the expander is preset for the desired size of the laser spot on the ground prior to the flight.

## 2.2 Laser receiver (RX)

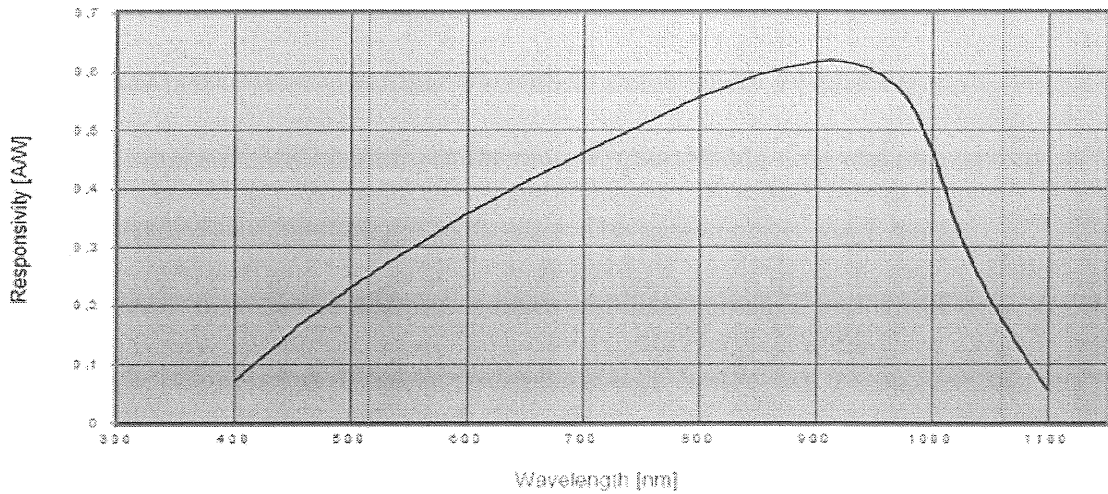


Figure 6: Responsivity curve of the photodiode used in the RX photodiode array.

*Image courtesy <http://silicon-sensor.com>*

Similar to the transmitter, the original receiver was the IF-VR2 unit manufactured by Industrial Fiber Optics. It was equipped with a single receiving photodiode that was very small, less than 1/16 of 1 square centimeter in size, as shown in Figure 7.

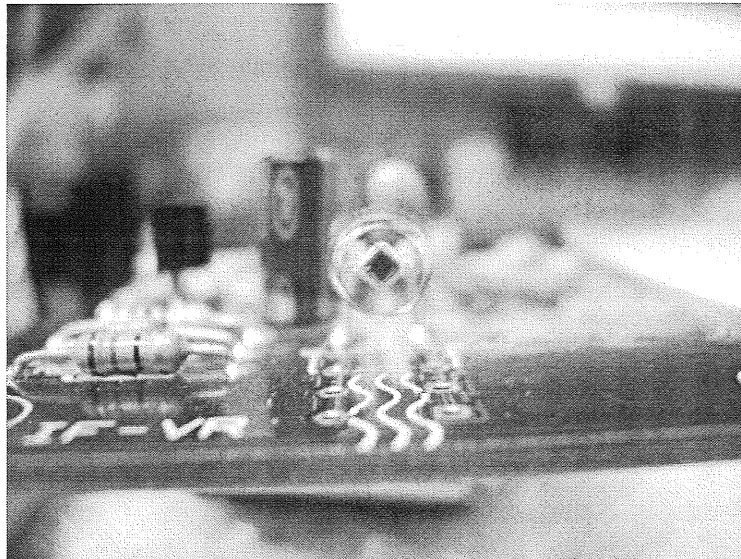


Figure 7: Original laser receiver with the receiving photodiode in front.

The black area on the diode observed in the picture is the actual silicon area that needs to be excited by the light source. This obviously was not large enough to perform long distance laser communications. Therefore, a new receiver board was designed and built based on the IF-VR2 board, but the receiver photodiode area was enlarged by connecting individual photodiodes in parallel. The receiver size was a major consideration that presented both advantages and disadvantages, and it will be discussed in detail. The enlargement of the receiver photodiode area makes it easier for the transmitter to point at and acquire communications, but at the same time, the nature of the silicon in the photodiode makes it more difficult to establish the connection. In addition, just as the desired laser light can be picked up more easily, the enlarged receiver area introduces a significant interference potential due to the ambient light being picked up by the photodiodes at the same time. Therefore, to account for the ambient light interference, a specially design optical bandpass filter was selected.

The circuit diagram of the photodiode receiver board is shown in Figure 8. The circuit was first designed and simulated in Electronics Workbench, and then it was built on a breadboard with an array of six photodiodes connected in parallel as shown in Figure 9. The array in Figure 9 was built by soldering six photodiodes on a copper covered board. In order to solder the six diodes, a small amount of soldering paste was used on the backside of each photodiode. Next, the photodiodes were tightly aligned on the copper board, pressed together, and placed in the oven for the solder paste to melt and to bond all together. Once the breadboard prototype proved to be working, the design from Electronics Workbench was transferred to the Ultiboard program for printed circuit

board (PCB) design. The design files from Ultiboard were sent to 4pcb.com for manufacturing.

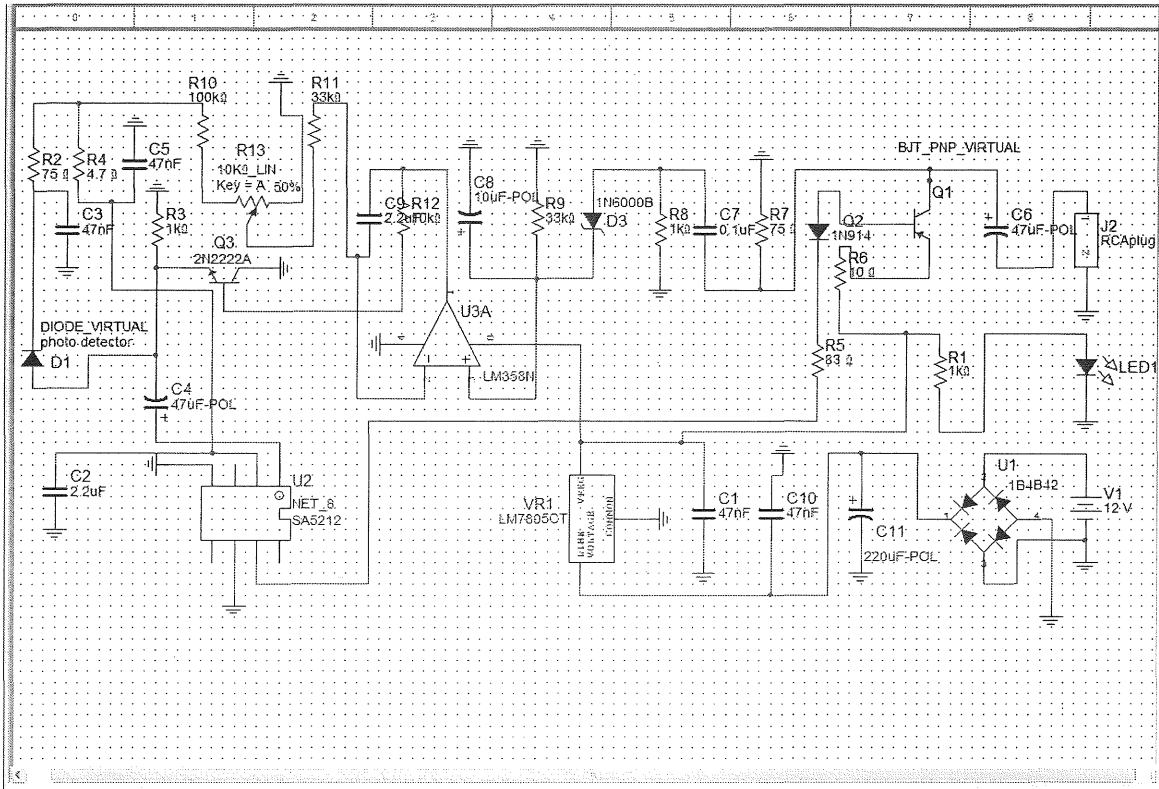


Figure 8: Laser RX diagram designed in Electronics Workbench.

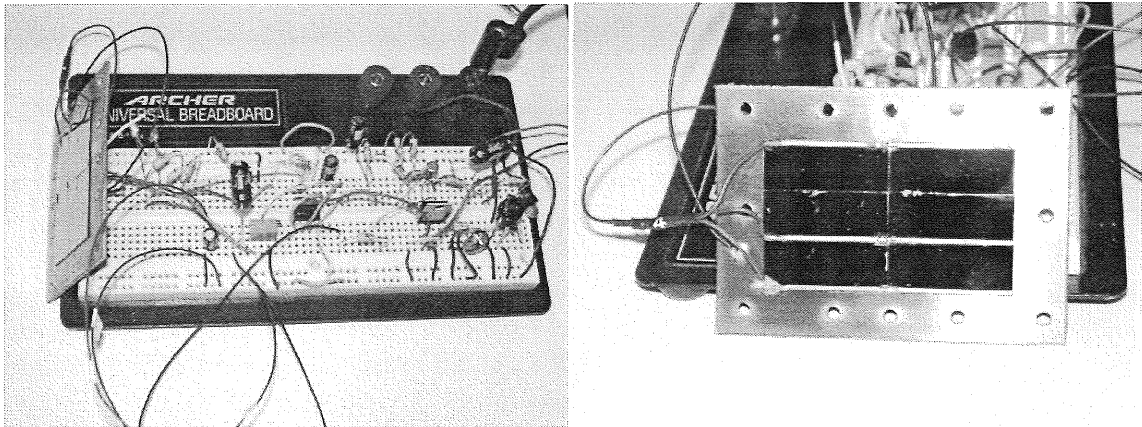


Figure 9: Laser RX circuit built on a breadboard with an array of six photodiodes.

Once the board arrived, it was populated with all components and the six photodiode array was connected. The working prototype is shown in Figure 10. After proving the functionality of this board, a custom 4.5cm × 4.5cm photodiode array consisting of sixteen photodiodes was ordered. The photodiode array was custom built according to our specifications by Pacific Silicon Sensor, Inc. [12], and it was then integrated into the laser RX PCB. The new photodiode array along with the PCB were placed in an aluminum box with dimensions 7in × 5in × 3in (WxDxH), as shown in Figure 11. The box comes with a lid, and the entire RX is battery powered for standalone application.

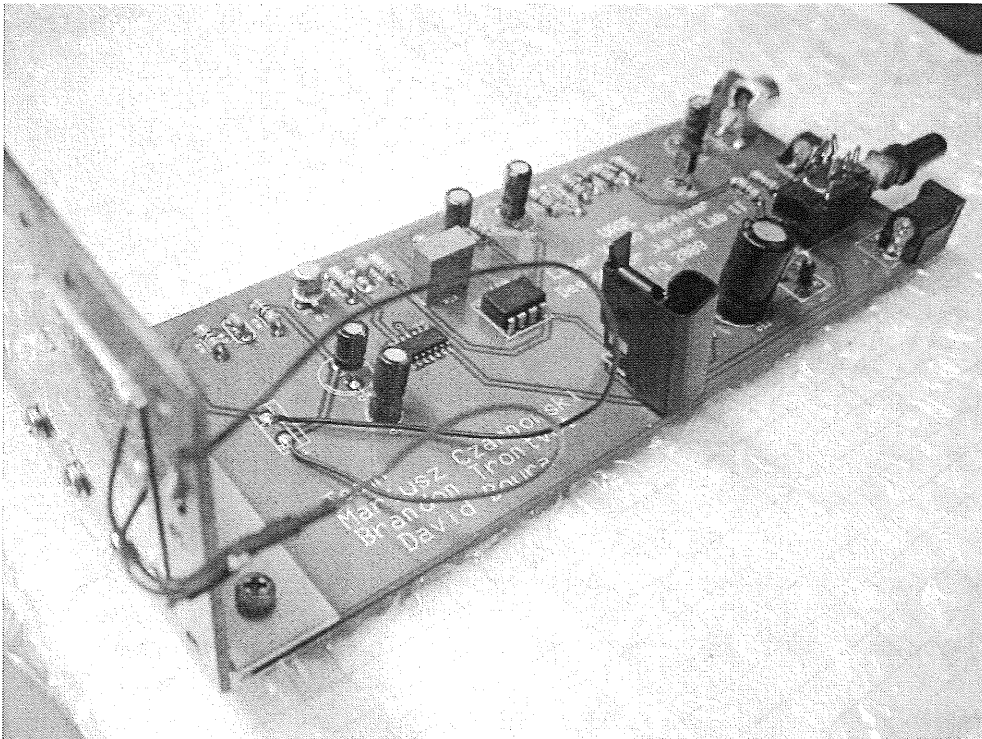


Figure 10: The PCB prototype of the laser RX.

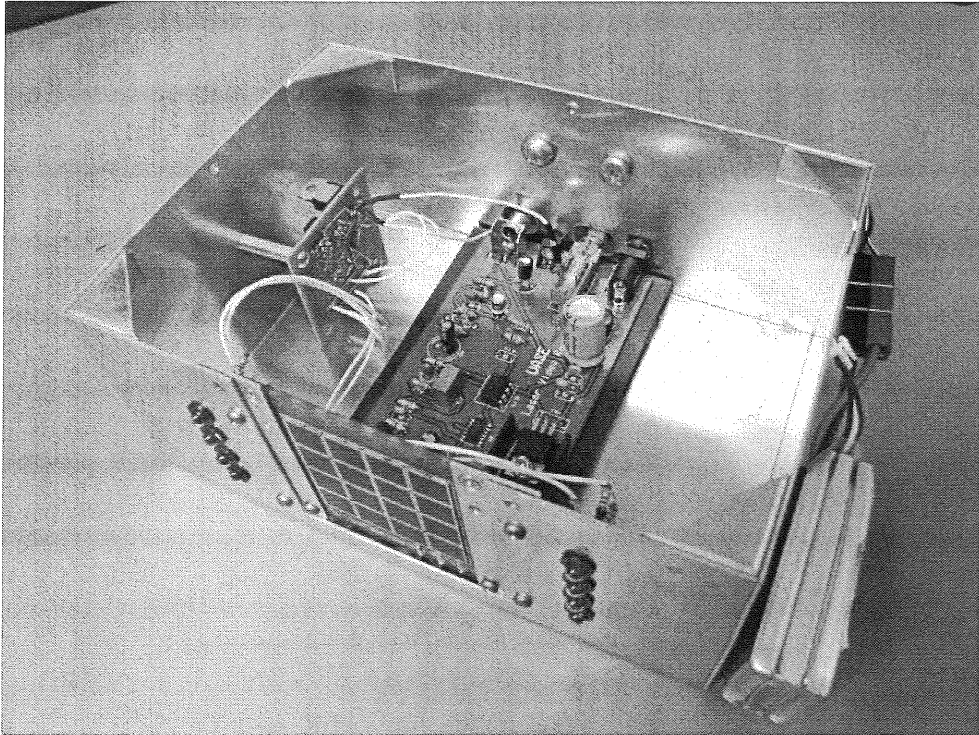


Figure 11: Laser RX box.

Note that there are eight near-infrared LEDs integrated into the RX box that were installed as a test for a machine vision-based tracking algorithm. The small circuitry in the upper left corner serves as a voltage regulating and pulsing circuit for the near-infrared diodes. By using a 555 timer and the appropriate resistor values, the LEDs can flash at our specified frequency.

As mentioned previously, the sensitivity of the photodiode at 800nm is near its peak, which significantly improves the responsiveness of the system when compared to the original laser diode that operated at 640nm. With such a large photodiode array, we were facing interference problems coming from the ambient light. Therefore, a bandpass optical filter from SpectroFilm [13] was installed in front of the photodiode array. The filter is a 6cm x 6cm bandpass filter with center wavelength of 808nm, and bandwidth of

70nm. The maximum angle of incidence (AOI) is 35degrees, with a typical center wavelength transmission of 85% as shown in Figure 12.

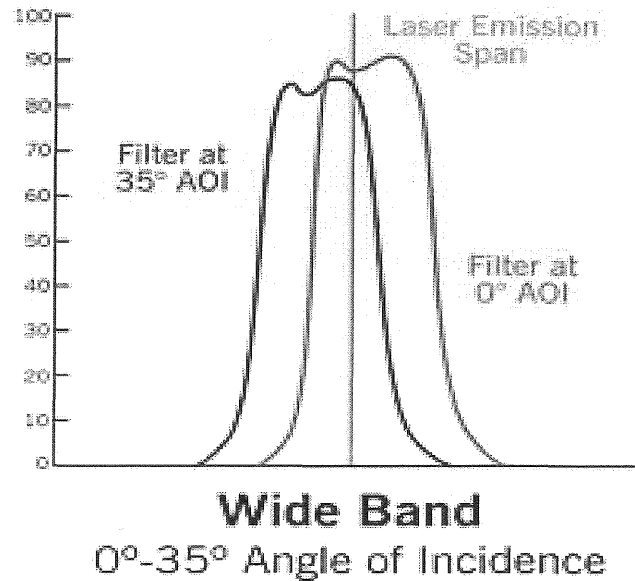


Figure 12: Bandpass filter specification.

According to the test results performed on the actual filter by the manufacturer, at 0degree AOI, the transmission is 86%, and at 30degree AOI, the transmission is 94%. Additional performance testing of the bandpass optical filter is discussed in the Section 5.1.3 of this thesis.



## CHAPTER 3

### TWO-AXIS GIMBAL POINTING SUBSYSTEM

In order to track the known GPS position of the laser RX on the ground, the airborne laser TX needs to be pointed at the target and maintained at that position for as long as possible. For this purpose, the laser TX was installed on the two-axis gimbal pointing system. The gimbal is controlled by the onboard computer running an automatic tracking algorithm. This chapter will discuss in detail the two-axis gimbal pointing subsystem.

#### 3.1 Flight computer

In order to accurately aim the laser transmitter towards the receiver in real-time, a computationally intensive automatic tracking algorithm has been developed and installed on the ELVIS flight computer. This computer must be very powerful, fast, small, and lightweight to be able to handle the near-real-time numerical calculations needed and to fit efficiently in the payload bay of the Super Hauler UAS. From our past experience in building payloads requiring computationally expensive algorithms in a small form factor, we knew that the PC104+ format computer was the right tool for the job. Therefore, the task was to find the most powerful, yet energy efficient PC104+ machine. The computer of choice was the system from Advanced Digital Logic [14]. This computer consists of an ADL945 [15] board that uses the Pentium Core 2 Duo 2.17GHz dual core processor, a

TRI-M HPS3512 [16] power supply board, 2GB of DDR2 RAM, a COM serial port expansion board, and an Intel 80GB solid state hard drive. All of these components are situated inside a Versa Tainer PC-104 computer box from Versa Logic Corporation [17]. The computer and the Versa Tainer box are shown in Figure 13. APPENDIX A contains the wiring schematic of the components.

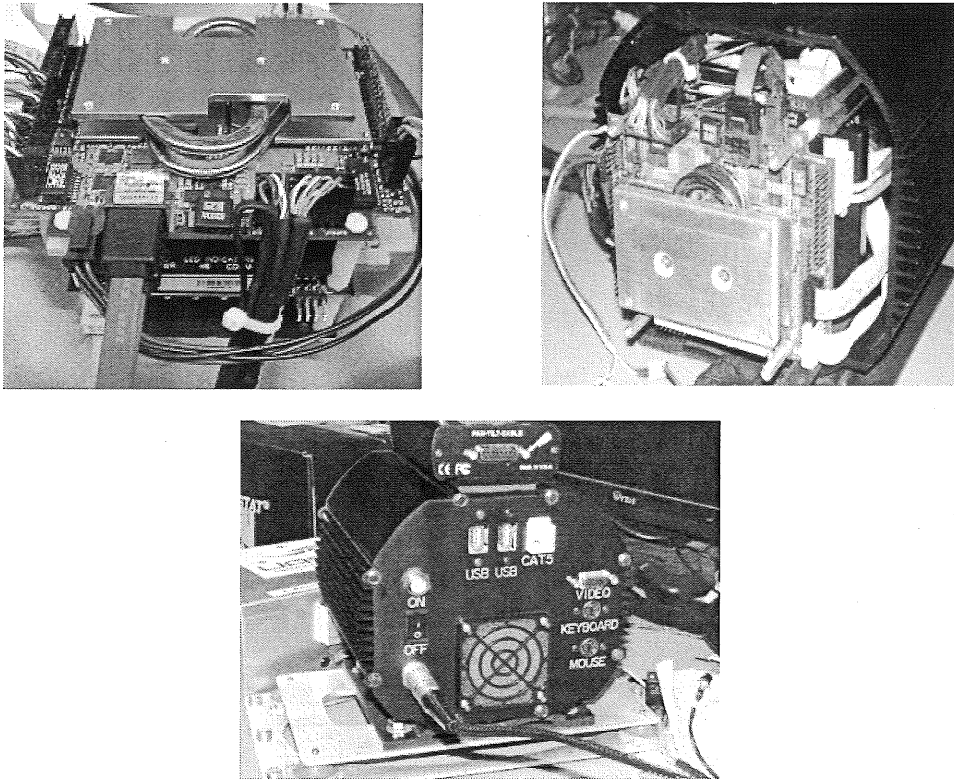


Figure 13: PC 104+ computer and its enclosure.

Upon receiving the computer and the Versa Tainer, there was a need for custom power cabling and a custom cooling system. According to the specifications supplied by ADL, all that the computer needed for cooling was an attachment of the heat pipe cooling system to the surface of the enclosure. That design was not deemed sufficient, so we decided to add three additional fans, one larger fan that sucks the air in and two smaller

fans that blow the air out. Because the Versa Tainer comes with generic endplates, all of the holes for fans, connectors, and connector descriptions had to be cut out using a computer numerical control (CNC) machine. The end plates and the fan placement are shown in Figure 14.

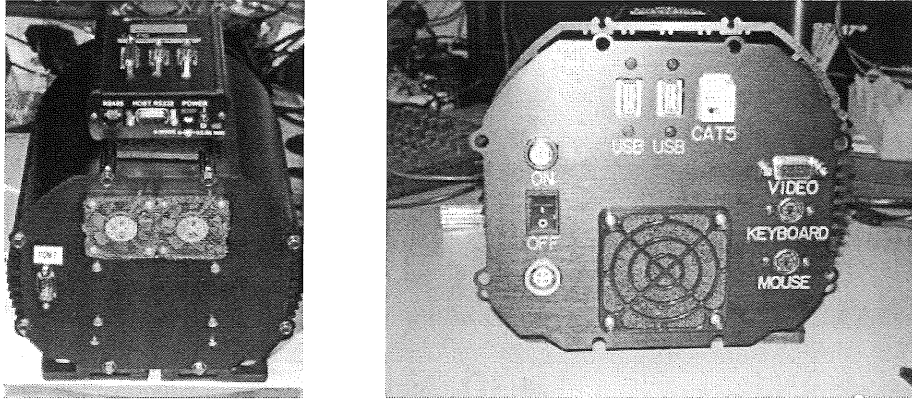


Figure 14: Versa Tainer end plates and fan placement.

Considering the fact that the computer is battery powered, a fuse along with the switch was installed. Figure 15 shows the wiring diagram of the fuse and the switch.

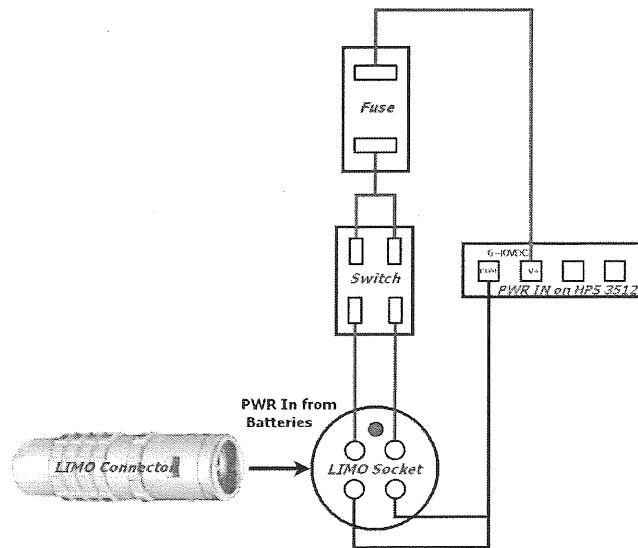


Figure 15: PC 104+ power input wiring diagram.

When we first ordered the computer, it did not have the serial port expansion board installed. It had two serial ports integrated into the ADL945 board, but we quickly realized that two serial ports were not enough. At first, we decided to use the available USB ports and to use USB-to-serial adaptors for all serial communication. This solution proved to be sufficient at first, but besides from delayed system performance from the adaptor, we also faced the need for more serial ports as the ELVIS project evolved and new components were added. Specifically, we needed a serial port to receive telemetry data from the autopilot, a serial port to communicate with the SONY block camera, and a serial port to send commands to the gimbal motor controller. Therefore, the MSMX104+ [18] serial port expansion board by Advanced Digital Logic was added to the computer stack. Figures 16 and 17 show the computer arrangement before and after adding the serial port expansion board. APPENDIX B contains wiring diagram and pin out of the serial ports on the MSMX104+ board.

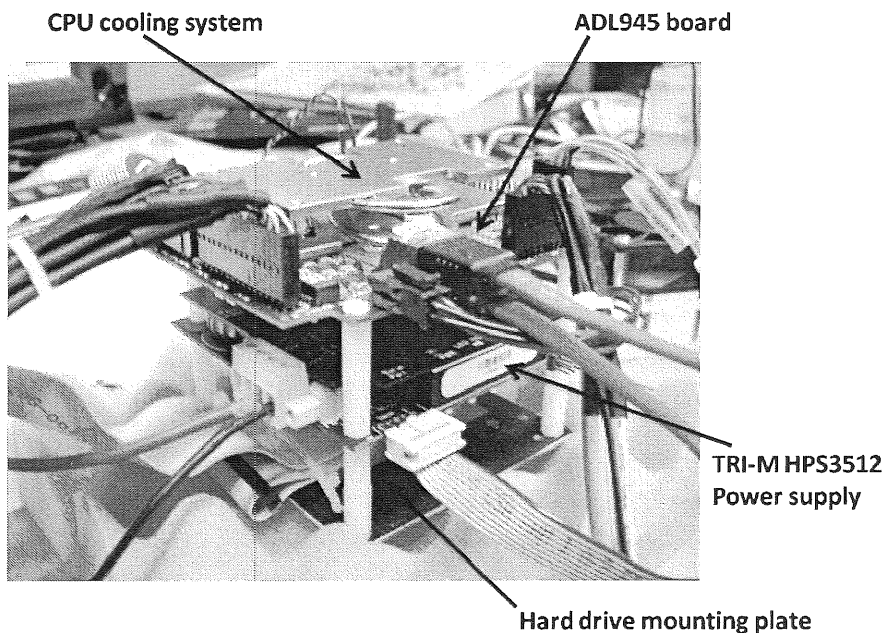


Figure 16: Computer stack before adding the serial port expansion board.

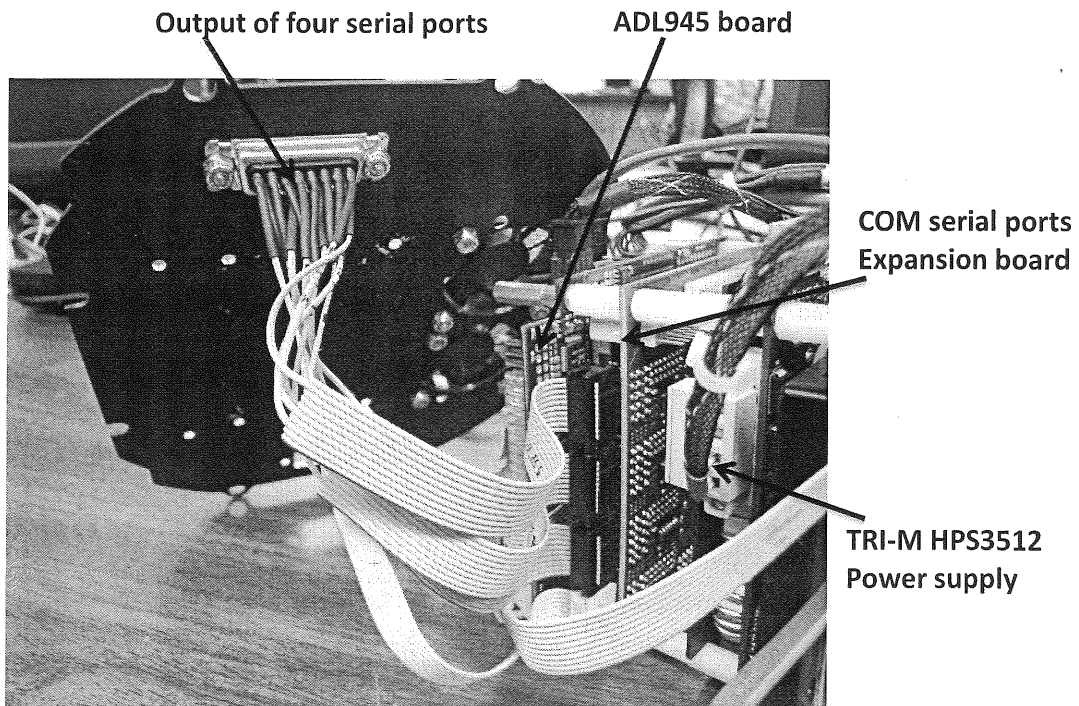


Figure 17: Computer stack after adding the serial port expansion board.

The addition of the serial port expansion board required some custom cabling. With the extra wires coming out of the expansion board, there was concern about the amount of room inside the computer enclosure. Also, there was not enough room on the end plates to drill an additional four holes for DB9 connectors. In order to accommodate for extra wires and connectors, the four serial ports were combined into one DB15 connector and mounted on the end plate as shown in Figure 17. Since each RS232 serial connection requires only three wires (TX, RX, and ground), we extracted only those three wires from each 10-wire ribbon cable coming from the serial port expansion board. Next, to have separate access to each of those four serial ports, a custom cable was built that had a DB15 connector on one end and four separate DB9 connectors on the other end, as shown in Figure 18.

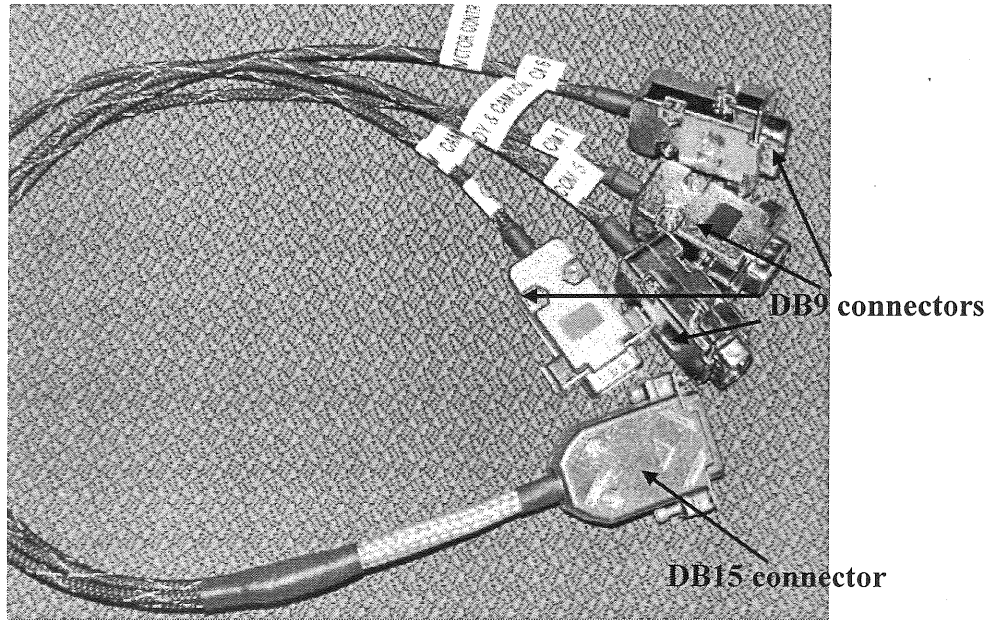


Figure 18: Custom built cable for four serial ports.

The DB15 end of the cable connects to the DB15 connector on the end plate of the computer enclosure, making four serial ports available for use in any application. The serial port expansion board actually has eight serial ports available, but due to lack of sufficient space inside the Versa Tainer enclosure, we had to limit the availability to four serial ports. Also, it should be noted that the board uses a switch for independent port transmission mode selection between TTL, RS232, and RS422/RS485. This gives the end-user the ability to disable a non-used port option by simply planning the switch in the OFF position and not supplying power to the serial port.

The ADL945 mother board has two internet interfaces, the LAN 1 and the LAN 2. The LAN 1 supports 10BaseT and 100BaseT compatible network components. The LAN 2 supports 10BaseT, 100BaseT, and 1000BaseT compatible net components. Both of these connectors come in a bundle with other connectors. LAN 1 comes with USB 1-4

and sound, and LAN 2 comes with USB 5-6. At first we were using the LAN 2 for our USB and internet purposes, but from the very beginning we had problems with internet connectivity. Therefore, we decided to extract the LAN 1 pins from the wire bundle and use it for our internet connection. The reason why we needed to extract the pins is that we are using only two USB ports and we do not use sound on our computer. This allows us to save room inside the Versa Tainer enclosure by eliminating unnecessary wiring. The pin out of the LAN 1 and LAN 2 connectors are included in APPENDIX C.

The current solid state hard drive (SSD) used in ELVIS is the Intel X25-M 80GB SSD. In order to keep the necessary overhead computing down to a minimal level, the operating system (OS) is the light version of Linux Gentoo. Even though we have had a number of problems installing the Linux Gentoo OS associated with a general lack of knowledge reconfiguring the Linux kernel, Gentoo has proven itself as a light and reliable OS. Linux in general is a very stable and efficient OS, which does not require a great deal of computational resources to perform at its best, and is known for its reliability. Our attempts of installing both Linux and the Windows OS on one hard drive caused us more problems than benefits. The problems lied in partitioning the hard drive and master boot record location. We finally decided to install the Windows OS on one SSD, and the Gentoo OS on a second SSD. The reason was that we were more familiar with Windows environment for software and hardware development. Once the software was working on the Windows platform, we then migrated the code into the Gentoo OS with the necessary changes made to accommodate the Linux environment.

One issue that we have had with the onboard computer is unexpected “freeze up” or crash of the computer. The screen would turn black for split of a second and then the

computer would become unresponsive. At that point the computer has to be restarted by means of powering it down using power switch. There was no particular reason or trigger that would cause this behavior, and we could never reproduce the crash in the lab. It is not an overheating issue. It was eliminated from the list by artificially overheating the system without. What has been noticed is that the voltage input to the mother board drops from required 5V-4.8V to below 4.5V. To improve the quality of the power input to the mother board from the HPS power supply, the connectors on the power line from the HPS to the mother board were re-soldered for better connectivity. This seemed to help the problem, because the onboard computer did not crash since. Another recommendation would be to replace the HPS power supply if the problem occurs again.

### 3.2 Gimbal control system

Finding the right gimbal system was a challenging task. The unit had to be DC powered, light weight, fast, and precise enough to correct for aircraft vibrations and to accurately point the laser TX over long distances. The actuator that was chosen is the model PTU-D46-70W precision Pan-Tilt Unit manufactured by Directed Perception [19], and it is shown in Figure 19.

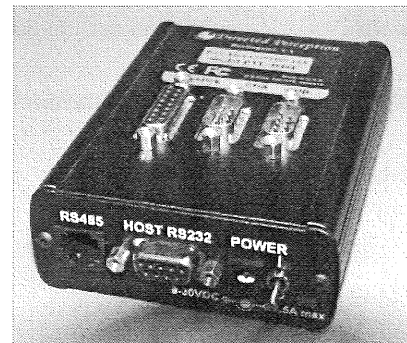
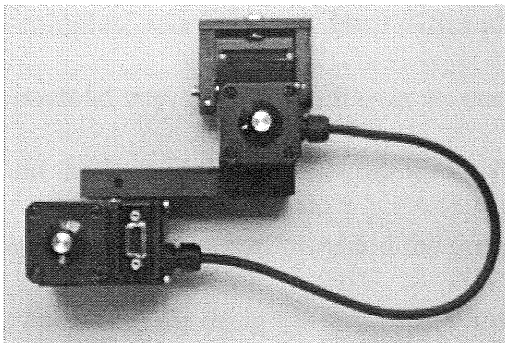


Figure 19: Two-axis pan-tilt gimbal system and motor controller.



Two rigid worm gear motors provide fast and accurate position control with a spinning speed of  $60^\circ$  per second and a step resolution of  $0.003^\circ$ . With a pan range from  $-159^\circ$  to  $159^\circ$  and a tilt range from  $-47^\circ$  to  $31^\circ$ , a significant range of vision is covered by the motion of this gimbal [20]. The gimbal controller communicates with the onboard computer via an RS232 interface and drives the two motors according to the pan and tilt angle commands issued by the onboard computer in real-time.

### 3.3 Mechanical mounting

The physical structure is a very important component of the ELVIS payload. This structure provides the platform on which everything is mounted. Therefore, if the mounting structure is not sufficient, the payload will not perform as designed. The desired qualities of the mounting system include being rigid, lightweight, stable, and having a small footprint. These desired characteristics are not difficult to obtain independently, but incorporating all of them together is very challenging. In fact, the mounting system needs to be rigid enough to keep from deflecting a rotational angle of  $0.018^\circ$  at a 3G (i.e., three times the force of gravity) load. The first aspect of the design that needed to be addressed was how to mount the gimbal system in the airplane so that it has complete rotational freedom. After placing the gimbal in the required location inside the payload bay, the room left over on each side totaled 2 inches. This left little space to mount the legs of the overall structure, which needs to be very rigid. Many designs were created, but the one that provided the greatest rigidity with the least amount of weight was chosen. This design is shown in Figure 20.

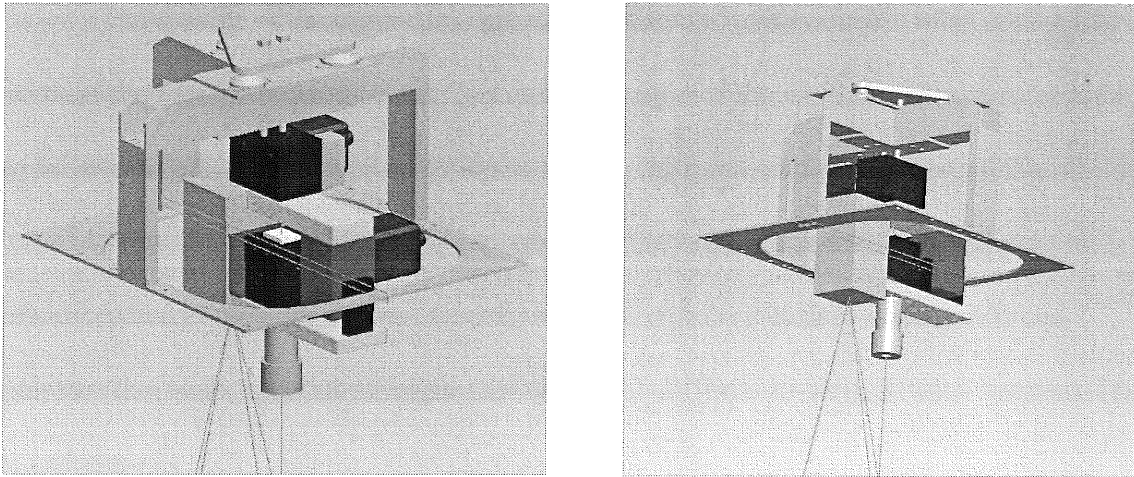


Figure 20: CAD representation of the mechanical mounting apparatus, the two-axis gimbal, laser transmitter, and EO camera.

The rigidity of the ELVIS payload was a major concern. After taking into account the designated flying altitude and the size of the photodiode receiver for the laser, the entire gimbal system could rotate no more than  $0.018^\circ$ . If it rotates beyond this limit, the laser will miss the receiver. To combat the rigidity issues, two of the three mounting points were located over the mounting rail in the payload bay. This ensured that there would be no deflections at the interface between the payload and the mounting rail. A continuous beam was placed between these two mounting points to provide the majority of the rigidity requirement. The third mounting point was located perpendicular to the main beam to provide torsional rigidity for the main beam. Finite Element Analysis (FEA) was performed on the current design, and it was found that at a 3G load, the structure would be within the deflection requirements. Hand calculations were performed to ensure that the FEA was correct. The percent difference between the two calculations was 1.2% [21].

The weight of the mounting structure was also a major concern after taking into account the rigidity requirements. The overall weight of the mounting structure needed to be less than five pounds. To fulfill the weight, stiffness, and ease of manufacturability requirements, 6061-T6 aluminum was chosen as the construction material. If time and resources had permitted, the best choice would have been a carbon fiber-reinforced polymer due to its superior strength-to-weight and stiffness-to-weight ratios compared to aluminum.

The stability of the mounting system was also a concern that needed to be addressed. The three-point mounting system was used exclusively in this design to ensure maximum stability with the least number of mounting points. Therefore, this would reduce the overall weight of the mounting system. From geometry, it can be shown that three points are required to define a plane. In order to increase the stability of the mounting system, any additional legs would need to be mounted in the same plane. If they were not in the same plane, it could actually reduce the stability of the mounting system. An example of this concept is the three-legged stool. A three-legged stool will never wobble while a four-legged stool can. To improve the stability even further, vibration dampers were used to reduce vibrations from the aircraft.

### 3.4 Automatic tracking algorithm

The automatic tracking algorithm is a crucial part of the entire system; therefore, a great deal of work and time has been put into refining the program to ensure precise pointing. The main considerations of the software are the coordinate system definitions, kinematic analysis, and software development.

### 3.4.1 Coordinate system definition

The tracking mechanism includes three separate coordinate systems, including the inertial coordinates, aircraft fixed coordinates, and gimbal coordinates. In this system, the inertial coordinates, shown in Figure 21, are defined as the x-axis in the North direction, the y-axis in the East direction, and the z-axis in the direction perpendicular to the plane formed by x-axis and y-axis. The aircraft fixed coordinates are defined at the center of mass of the aircraft: the x-axis is aligned with the heading direction, the y-axis is perpendicular to the x-axis and points to the right side of the aircraft, and the z-axis is perpendicular to the plane formed by the x-axis and the y-axis. The gimbal coordinates are defined with the x-axis aligned with the zero position of pan, and the y-axis aligned with the zero position of tilt.

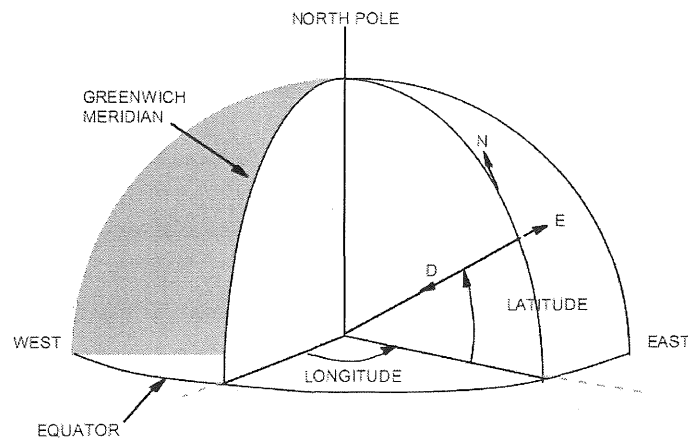


Figure 21: Orientation of inertial coordinates.

### 3.4.2 Kinematics analysis of the system

With multiple coordinate systems, vector operations cannot be performed if the vectors are defined by different coordinate systems. Therefore, coordinate transforms are

needed. The first transform needed for this analysis is a transform between the inertial coordinates to the aircraft fixed coordinates. In this case,  $\phi$  is the heading angle, or yaw, that corresponds to a rotation about the z-axis of the aircraft fixed system,  $\theta$  is the pitch angle and is a rotation about the y-axis of the aircraft fixed system, and  $\psi$  is the roll angle corresponding to a rotation about the x-axis of the aircraft fixed system. The order of rotations for this transform is  $\psi$ ,  $\theta$ , and then  $\phi$ . In this case, the system inputs are aircraft location in the inertial coordinate system including latitude, longitude, and altitude (GPS information),  $P$ ; aircraft attitude (inertial measurement unit information, roll, pitch, and yaw),  $A$ ; the predefined ground target location in inertial coordinate system (GPS information),  $T$ ; and the offset,  $G_0$ , or the difference between the onboard GPS device location to the gimbal location.

From aircraft coordinates to aircraft body-fixed coordinates, a rotation matrix  $R_a$  is needed, defined as

$$R_a = \begin{bmatrix} c\psi c\theta & s\psi c\theta & -s\theta \\ -s\psi c\phi + c\psi s\theta s\phi & c\psi c\phi + s\psi s\theta s\phi & c\theta s\phi \\ s\psi s\phi + c\psi s\theta c\phi & -c\psi s\phi + s\psi s\theta c\phi & c\theta c\phi \end{bmatrix}. \quad (1)$$

The aircraft body-fixed coordinate,  $P_a$ , is then given as

$$P_a = R_a P. \quad (2)$$

The aircraft body-fixed coordinate of the gimbal can be found by subtracting the gimbal offset from the aircraft body-fixed coordinates,

$$G_a = P_a - G_0. \quad (3)$$

To obtain the gimbal location in the inertial coordinate system, the inverse of the aircraft rotation matrix is multiplied by the aircraft body-fixed coordinates of the gimbal system,

$$G = R_a^{-1}G_a. \quad (4)$$

The line-of-sight vector is defined as the difference between the gimbal location and target location, both given in inertial coordinates:

$$D = T - G = \begin{bmatrix} \Delta x \\ \Delta y \\ \Delta z \end{bmatrix}. \quad (5)$$

The line-of-sight vector in aircraft body-fixed coordinates is obtained by multiplying  $D$  by the aircraft rotation matrix,  $R_a$ :

$$D_a = R_a D = \begin{bmatrix} \Delta x_a \\ \Delta y_a \\ \Delta z_a \end{bmatrix}. \quad (6)$$

The final rotation transforms the line-of-sight vector in aircraft body-fixed coordinates into the gimbal body-fixed coordinate system. This is accomplished by multiplying the gimbal rotation matrix  $R_g$ , where  $\alpha$ ,  $\beta$ , and  $\gamma$  are the actual rotation angles of the gimbal system, by the line-of-sight vector in aircraft body-fixed coordinates:

$$R_g = \begin{bmatrix} c\gamma c\alpha + s\gamma s\beta s\alpha & c\gamma s\alpha - s\gamma s\beta c\alpha & s\gamma c\beta \\ -c\beta s\alpha & c\beta c\alpha & s\beta \\ -s\gamma c\alpha + c\gamma s\beta s\alpha & -s\gamma s\alpha - c\gamma s\beta c\alpha & c\gamma c\beta \end{bmatrix}. \quad (7)$$

$$D_g = R_g D_a = \begin{bmatrix} \Delta x_g \\ \Delta y_g \\ \Delta z_g \end{bmatrix}. \quad (8)$$

Since the y-direction of the gimbal system should always align with the pointing direction, the angle rotation in the z-direction can be ignored. By placing all the equations and rotation matrices in the right sequence, the angle solution can be derived as a closed-form solution [22]:

$$\alpha = \tan^{-1} \left( \frac{-(c\psi c\theta)\Delta x + (s\psi c\theta)\Delta y + (-s\theta)\Delta z}{(-s\psi c\phi + c\psi s\theta s\phi)\Delta x + (c\psi c\phi + s\psi s\theta s\phi)\Delta y + (c\theta s\phi)\Delta z} \right) \quad (9)$$

$$\beta = \tan^{-1} \left( \frac{-(s\psi s\phi + c\psi s\theta c\phi)\Delta x + (-c\psi s\phi + s\psi s\theta c\phi)\Delta y + (c\theta c\phi)\Delta z}{s\alpha(c\psi c\phi)\Delta x + (s\psi c\theta)\Delta y + (-s\theta)\Delta z - c\alpha(-s\psi c\phi + c\psi s\theta s\phi)\Delta x + (c\psi c\phi + s\psi s\theta s\phi)\Delta y + (c\theta s\phi)\Delta z} \right) \quad (10)$$

### 3.4.3 Software implementation

Three major tasks need to be executed in sequence to achieve one tracking motion. First, a serial communications link must be established between the flight computer and the Cloud Cap Technology Piccolo II autopilot system. According to the autopilot system status, the flight computer receives and parses the differential GPS and IMU information of the aircraft from the telemetry file [23]. Table 1 summarizes the accuracy differences in DGPS and IMU data between the TELEMETRY\_HI\_RES and TELEMETRY\_LO\_RES files.

Table 1: Summary of DGPS and IMU data.

	TELEMETRY_HI_RES	TELEMETRY_LO_RES
DGPS Data	32-bit signed integer, in milli-arcseconds	24-bit unsigned integer, 2.4 meters at the equator
IMU Data	16-bit signed Euler angle in 1/10000 <sup>th</sup> radians	8-bit signed integer angle, in units of (360/256) degrees for yaw and roll, and (180/256) degrees for pitch

Second, the photodiode receiver location, including latitude, longitude, and altitude, as well as the gimbal offset values in three axes need to be input to the tracking algorithm manually. Once the aircraft location and motion information are retrieved from the telemetry file, the gimbal control algorithm reads in the data and computes the gimbal pan and tilt angles at a rate of 20Hz to compute the line-of-sight vector between the modulated video laser transmitter and photodiode receiver following the kinematics analysis described in Section 3.4.2.

Third, the calculated gimbal pan and tilt angles must be converted into a position by taking into account the motor resolution factors. A custom C program formats commands by following the syntax of pan and tilt unit control commands. For example, the command PP-3000 causes the pan motor to rotate to position -3000 [24].

The gimbal control algorithm was designed using MATLAB scripts and C source code integrated into an Embedded MATLAB interface and coupled with MATLAB Real-Time Workshop to automatically compile and generate an executable program. The diagram in Figure 22 describes the Embedded MATLAB task sequence shown in Simulink.

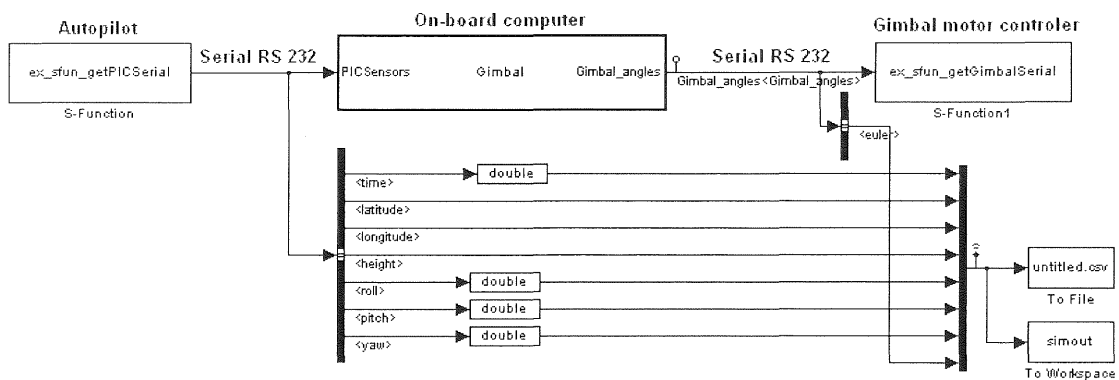


Figure 22: Simulink block diagram for Embedded MATLAB.



### 3.5 Joystick control

To further expand on the capabilities of machine vision-based tracking, manual joystick control of the pointing gimbal was developed. The idea is to manually point the gimbal at the target while using the EO camera mounted parallel to the laser TX as visual feedback. Once the camera is aligned with the target, a machine vision-based tracking method can take over for fine adjustments. Joystick control will also be useful when verifying the correct operation of the TX/RX components of the system by manually pointing the laser TX at the RX on the ground. In addition, the zoom of the camera and its near IR filter can be also controlled through the joystick. The joystick selected is the Wingman Joystick by Logitech, as shown in Figure 23.



Figure 23: Joystick used to manually control the gimbal and SONY camera. *Courtesy:* [http://ecx.images-amazon.com/images/I/414X2Z0A7TL.\\_SL500\\_AA280\\_.jpg](http://ecx.images-amazon.com/images/I/414X2Z0A7TL._SL500_AA280_.jpg)

The software used for controlling the gimbal and the camera is written in MATLAB. It consists of two separate programs, one for the ground-based computer and

the other for the onboard airborne computer. APPENDIX D contains the ground-based computer code and APPENDIX E contains onboard computer split code. The code on the ground-based computer sends both the gimbal commands and the camera commands via serial port as one string, 22 bytes in length. This command is fed into the autopilot ground station and sent through the 900MHz link to the onboard autopilot unit and passed through a serial port to the onboard computer. Here, the onboard computer code splits this long message into two separate commands, one for gimbal control and one for camera control. Each of these commands is sent to a separate serial port to its destination. Each button on the joystick has an assigned functionality. After running the MATLAB code on the ground-based computer, a window pops up giving the list of button functions as shown in Figure 24.

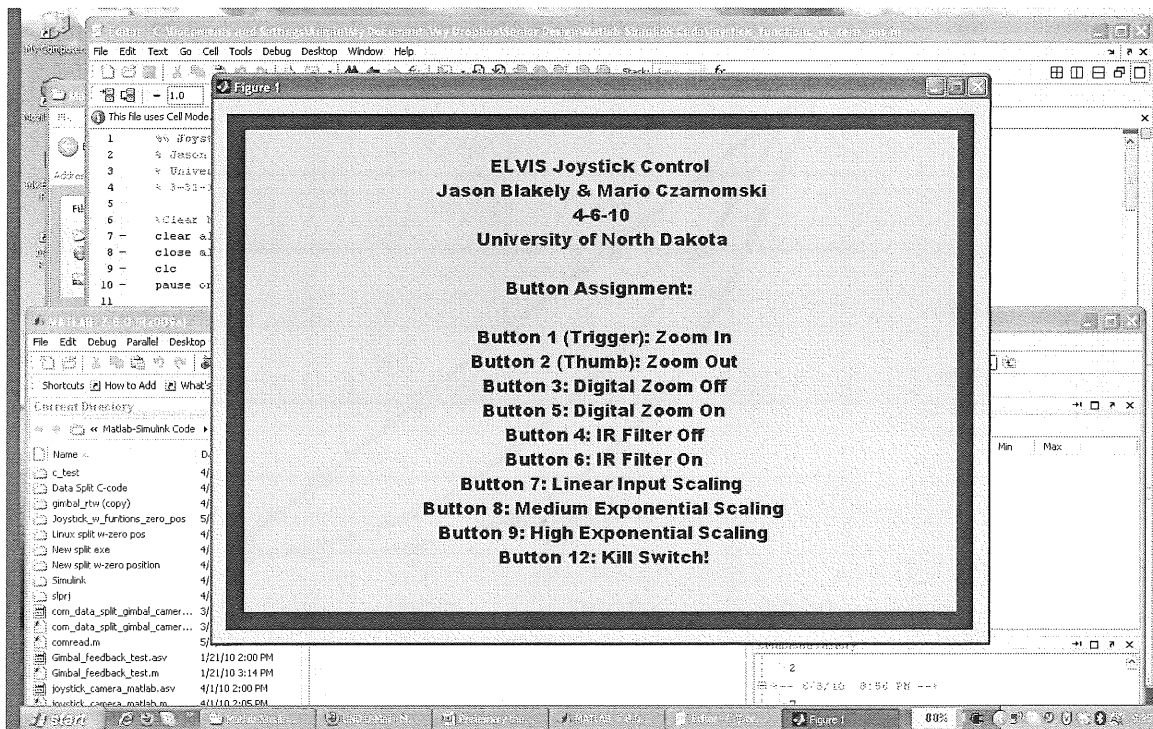


Figure 24: Snapshot of the MATLAB pop up window with the joystick buttons function assignment.

During joystick control, the gimbal is operated in a velocity control mode compared to position control mode while under control of the automatic tracking algorithm. Velocity mode enables smoother gimbal rotation and therefore more precise pointing and tracking. To further improve the precision of pointing during joystick operation, an exponential velocity control was implemented. This approach permits more precise operation of the gimbal in its lower speeds, giving more precision in pointing. In other words, large movements of the joystick in the lower range translate into slow movements of the gimbal. At the same time, full gimbal velocity is available upon full joystick deflection. The three functions used for controlling the gimbal with the joystick are shown in Figure 25.

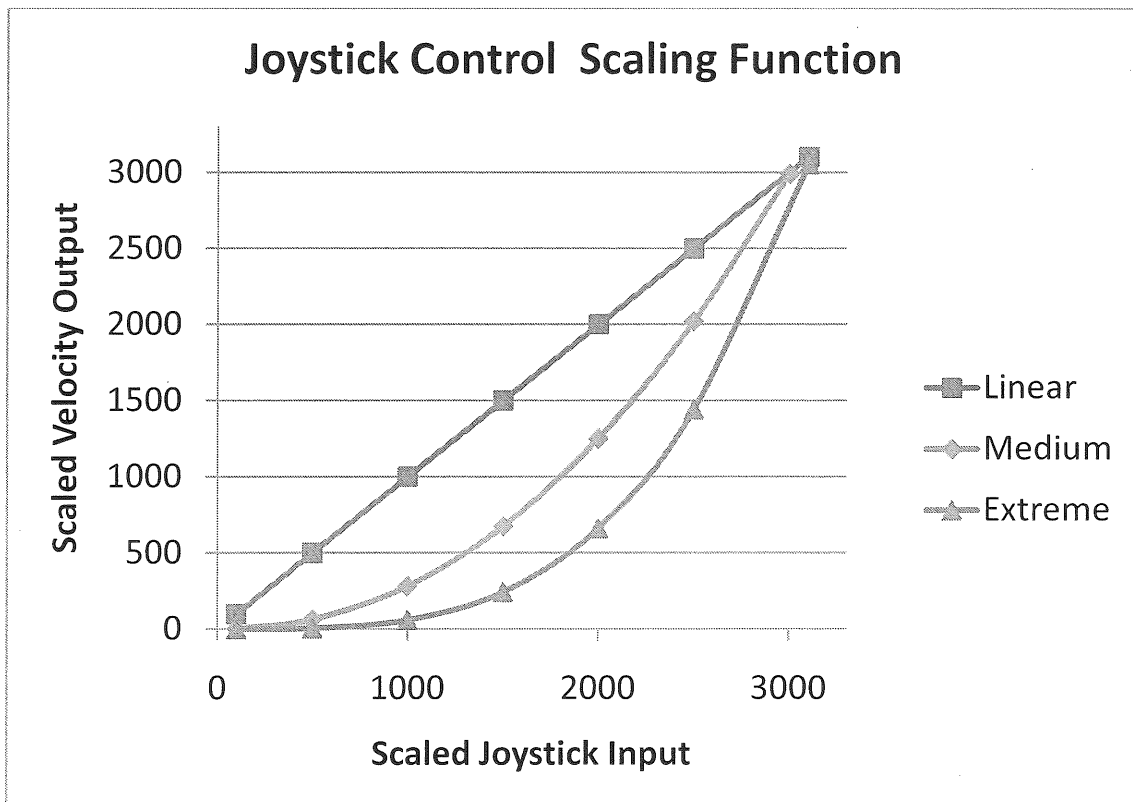


Figure 25: Three functions available for the joystick velocity control of the gimbal.

The user can switch between all three of the functions at any time by simply pushing the appropriate button on the joystick. The button assignment is displayed for the user every time the program is executed, as shown in Figure 24. For example, a joystick input of 1000 (the deflection of the joystick approximately one-fourth of its maximum deflection) will result in a velocity of 1000 positions per second in linear function mode, but the same joystick deflection will result in a velocity of about 250 positions per second for the medium function setting and only 100 positions per second for the extreme function setting.

## CHAPTER 4

### STEPS IN THE INTEGRATION PROCESS

Integrating all the components that comprise the ELVIS payload is not an easy task. Quite often, the components work by themselves, but when interfaced with other subsystems, they simply refuse to cooperate. This chapter will present the steps in the process of integrating the ELVIS subsystems, as well as the difficulties and challenges encountered.

#### 4.1 Crucial system components

Crucial system components can be divided in two subgroups: the airborne components and the ground-based components. The airborne components had to be integrated into the Super Hauler UAS, whereas the ground-based components had to be interfaced with each other and, depending on the mode of operation, into the autopilot ground station.

##### 4.1.1 Airborne components

The list of the airborne components consists of the following devices: laser TX, gimbal unit, SONY block camera, gimbal/components mount, forward-looking camera (source of the video being transmitted over the laser), on-board PC104+ computer, and

the Piccolo II autopilot. This last device is separate from the ELVIS payload, but it is crucial in the successful operation of the system. All components have to work seamlessly in order for the ELVIS to successfully transmit video.

Laser TX is based on the commercially available IF-VL30 unit from Industrial Fiber Optics. The board was retrofitted with the new, more powerful 100mW red laser diode at 660nm. For ease of rotating the laser and integrating the TX onto the gimbal, the laser diode head contacting the laser diode was removed from the TX board and installed in a convenient location on the gimbal to ensure balanced rotation. Extension wires from the TX board to the laser diode head were used in this case. In addition, the laser diode head was housed inside a custom manufactured aluminum enclosure to facilitate mounting the laser beam expander, as shown in Figure 26.

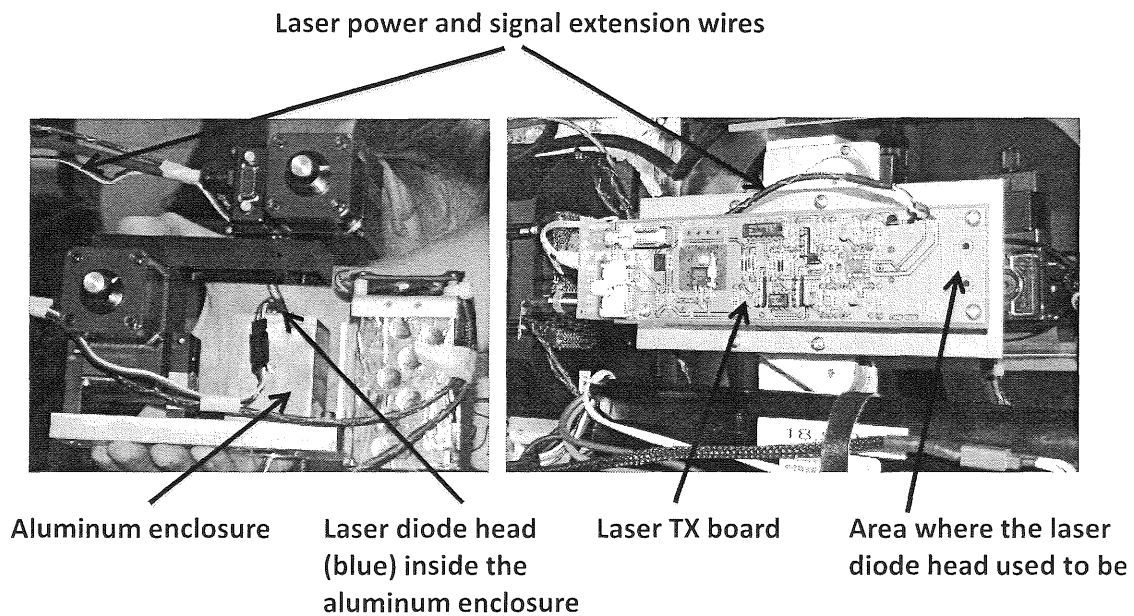


Figure 26: Laser TX board with aluminum laser diode head enclosure and extension wires.

The design of the aluminum enclosure required us to take into account that the laser beam expander will be mounted in front of the laser head. One of the threaded adapters was inserted and glued inside the enclosure. This allows the beam expander to be screwed in as needed. Also, special attention was paid to make sure that once screwed in, the expander's 2.5mm entrance aperture was as close to the focal point of the laser diode as possible. This ensures that the entire laser beam enters the expander and there is no loss.

The PTU-D46-70W two-axis gimbal system was chosen after an extensive trade study. Its low price and specifications met our preliminary requirements: low weight, DC powered, capable of lifting >5lbs, with a relatively fast response time. It was not quite specified what the required speed of the motors, their precision, or pan and tilt maximum angles should be, because it was all new to us and in a way we were experimenting. More on the gimbal selection will be discussed in Section 6.4 of this thesis. Before any integration and gimbal mount manufacturing took place, the gimbal along with the Super Hauler payload bay were modeled in a CAD program to ensure unimpeded rotation and operation of the gimbal within the payload bay. A detailed description of the process is described in Section 3.4. Once modeling proved to be successful, the gimbal mount was manufactured and assembled in the lab. The image of the mount itself within the payload bay is shown in Figure 27.

The entire structure rests on the aluminum rails that run along the payload bay. The payload is secured to the rails using quarter turn fasteners visible in Figure 27. The two vibration isolation mounts (the third one is missing in the picture) are strategically placed so that they provide a stable, three-point vibration isolation support.

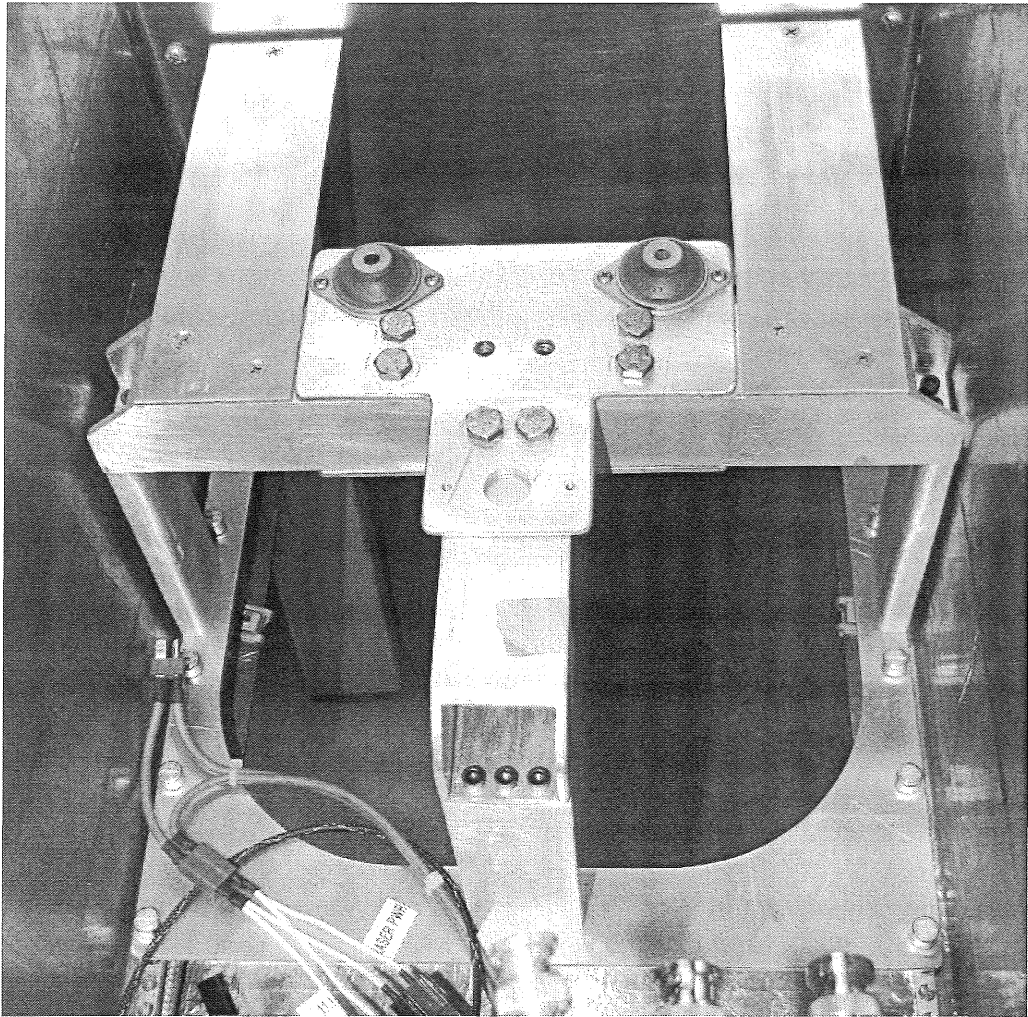


Figure 27: ELVIS payload mount inside of the Super Hauler payload bay.

These vibration isolation mounts absorb high frequencies produced by the Super Hauler engine and also work to cushion the payload during landings. A triangular shaped aluminum plate is placed on top of three vibration mounts, and two long bolts are secured to the center of the triangular plate. Those two bolts serve as the mounting point for the gimbal. When all parts are assembled, the gimbal is basically suspended from the triangular plate that rests on the vibration mounts. Figure 28 shows the mounting configuration of the gimbal.



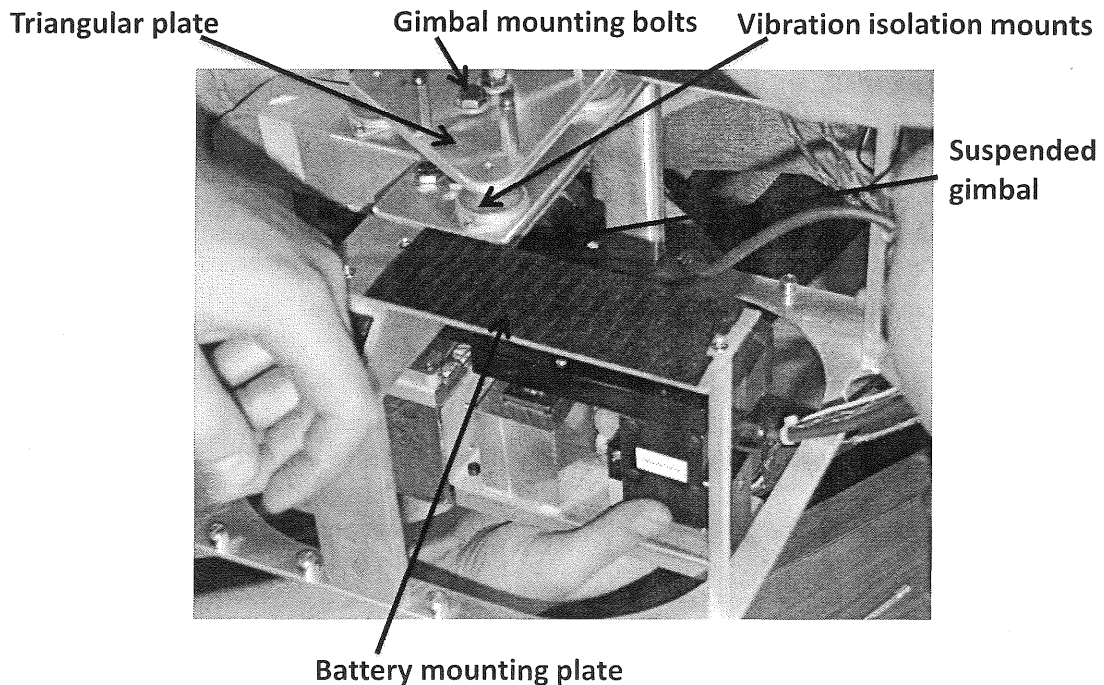


Figure 28: Assembly of gimbal mount and gimbal system.

The final piece of the gimbal assembly is the SONY block camera, which was mounted parallel to the laser diode aluminum enclosure. Custom cabling was also built to ensure reliable powering of the camera, video transmission through the 1.7GHz RF transmitter available onboard the UAS, and remote camera control via serial port accessible on the camera. Using this serial connection, we are able to control the optical and digital zoom, turn the near infrared (IR) filter on or off, adjust the iris, and set many other optical settings. The serial communications is available through the 900MHz RF autopilot link. The serial port from the camera is plugged into one of the five serial ports on the autopilot. The control commands are sent over the autopilot RF channel from the notebook computer connected to the serial port on the autopilot ground station, and then passed through to the SONY block camera. The laptop on the ground can control the

camera in two ways. One way is to run the SONY camera software, where all the optical and fine tuning options are available. The other way of operating the camera is through the use of the joystick and the custom MATLAB code. When controlled by the joystick, the available commands are optical and digital zoom, and turning the near IR filter on or off.

The “brain” of the airborne components is the PC 104+ onboard computer. The computer specifications are described in Sections 3.1. The unit is first enclosed inside the Versa Tainer aluminum enclosure, and it is then bolted down to the aluminum plate. This plate sits on four vibration isolation mounts that in turn are attached to the payload bay mount aluminum plate as shown in Figure 29. The vibration mounts serve the same purpose as the gimbal mounts: high frequency cancellation and shock absorption during landing. The payload bay mount plate is secured to the rails running along the payload bay using six quarter turn fasteners.

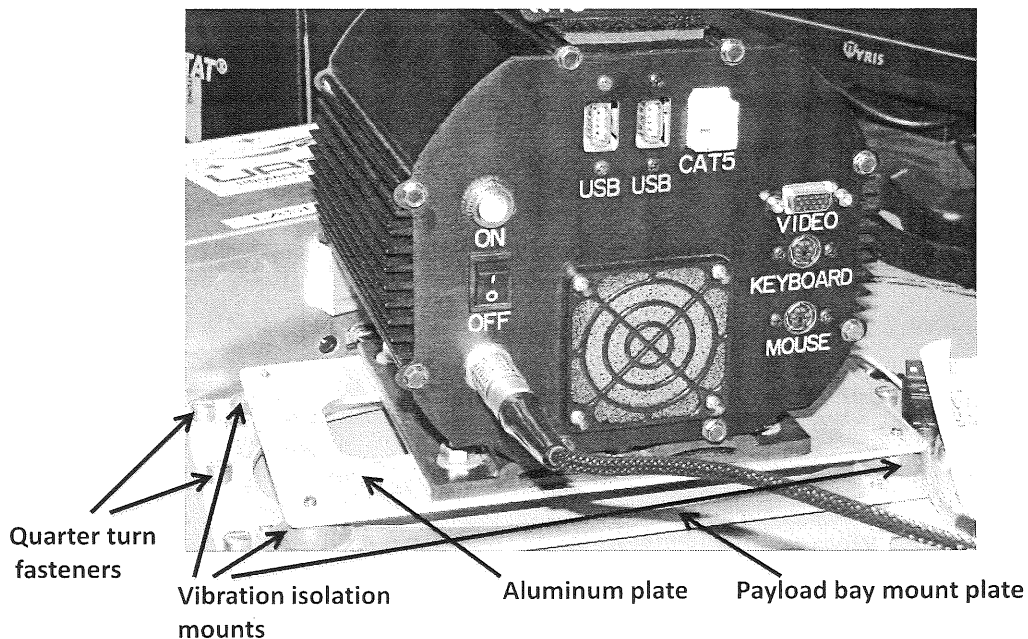


Figure 29: Mounting configuration of the PC 104+ onboard computer.

The computer interfaces with external components via five available serial ports. Four of these ports can be hardware configured as TTL, RS232, or RS422/485, but in the current cable configuration only RS232 is available, because the DB9 connectors have only three wires installed suitable for RS232. Communications between the computer and the external components is crucial, and therefore a significant amount of time was taken to ensure correct operation of the serial ports. They were first tested in the Windows OS environment, and then, after ensuring that the hardware was operating correctly, the serial ports were configured and tested in the Gentoo Linux OS. In order for the gimbal to move, position commands are sent via the serial port from the computer to the motor controller unit that currently sits on top of the computer enclosure. Next, the motor controller sends the commands to the gimbal motors through the special cable supplied with the gimbal.

#### 4.1.2 Ground-based components

Currently, ground based components consist of the laser RX that is mounted on a stationary tripod, a video monitor, and a laptop computer.

The laser RX is based on the commercially available IF-VR2 unit from Industrial Fiber Optics. More details on the unit can be found in Section 2.2 of this paper. The receiver is mounted on the tripod using a standard camera bolt, with the array pointing straight up. Upon receiving laser light from the transmitter, the signal is demodulated and sent over the RCA cable to either the small SONY display or to our universal payload ground station, where we have capabilities to record the transmitted video onto the laptop computer. In addition, the 1.7GHz video signal coming from the SONY block camera on

the payload is received by the universal payload ground station and can be viewed on one of the available displays or recorded on the notebook computer for the future reference. In order record video on the notebook computer, the signal has to be passed through a digital video recorder (DVR) unit. The DVR performs the analog -o-digital conversion of the signal so that it can be recorded by the DVR software on the laptop.

#### 4.2 UAS platform

The UAS platform used to test ELVIS is the Super Hauler aircraft, custom built by Bruce Tharpe Engineering (BTE). The aircraft is capable of hauling relatively large payloads, is modifiable, easy to operate, and has an excellent flight duration. These attributes make the Super Hauler an ideal platform for our research purposes. The airframe is lightweight yet strong, and is constructed from easy-to-work-with materials such as balsa, plywood, and aluminum. Since a variety of components are installed onboard the airframe, it is crucial for us to be able to modify the payload bay to accommodate our custom equipment. The airplane's powerful 9.8Hp, two-stroke, 100cc engine and large 12foot wing span allows it to lift a payload with a weight of approximately 25-30pounds. The rectangular payload bay has dimensions of 22in × 11.5in × 13in (L×W×D), which provides a significant volume for custom payload development. The aircraft and its payload bay are shown in Figure 30.

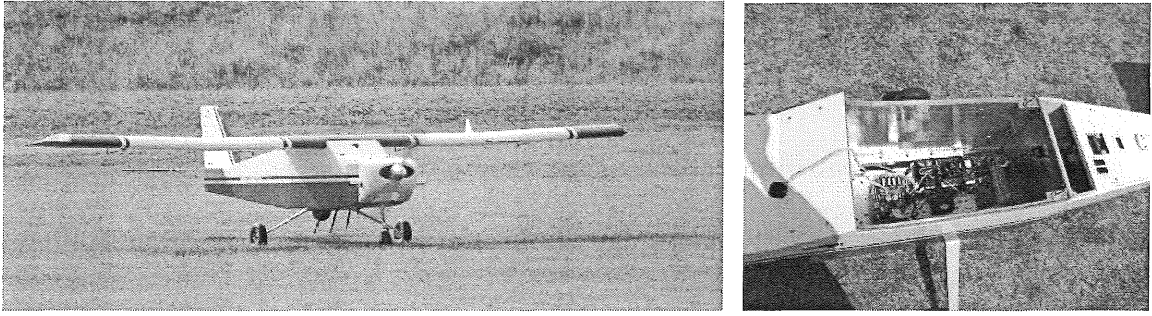


Figure 30: Super Hauler UAS and its payload bay.

### 4.3 Autopilot integration

An operational, well-tuned autopilot is a crucial element of all the payload test flights and missions that we perform. As a matter of fact, the autopilot quite often becomes such a critical component of the payload where a payload cannot operate without the interfaces an autopilot offers. In this section, we will discuss the process of autopilot integration into the Super Hauler UAS, and the benefits that came from this experience.

#### 4.3.1 Steps in the process of integration

The entire enterprise was a multi-step process that required a systems engineering approach, which began with the collection of all crucial parts and components. The list consists of the aircraft, autopilot, ground station, GPS, 900 MHz antennas, and cabling, as shown in Figure 31. A custom designed aircraft was purchased from BTE due to the specific requirements regarding the material used for the airframe and the size and shape of the payload bay. The aircraft needed to be easily modifiable, have a rectangular payload bay, and be capable of carrying payloads of up to 30lbs in weight.

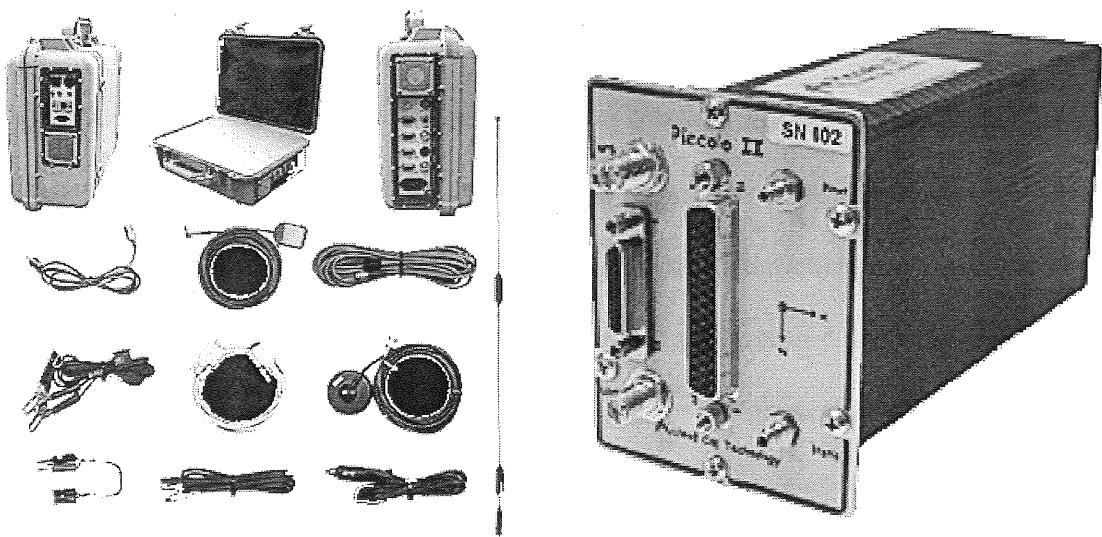
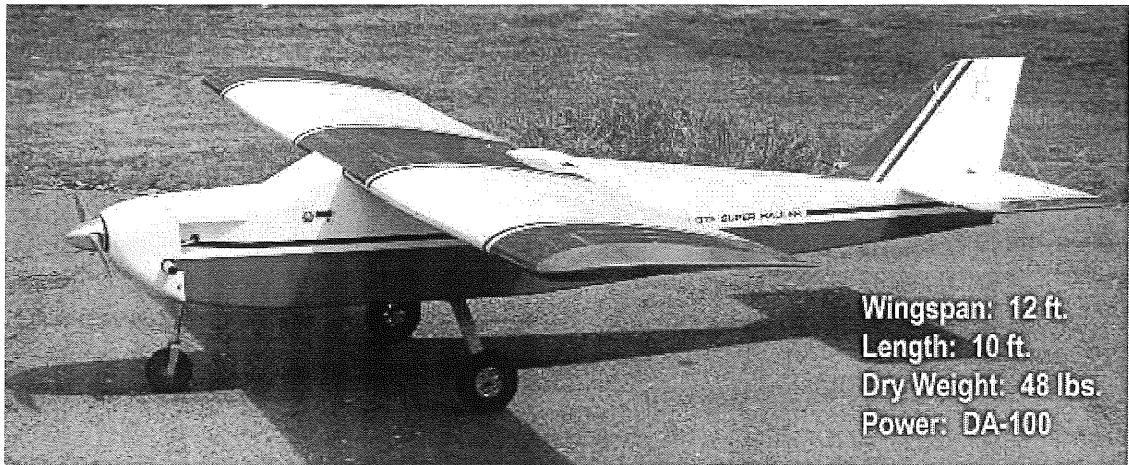


Figure 31: UAS autopilot system components. *Courtesy: [www.cloudcaptech.com](http://www.cloudcaptech.com)*

The choice for the autopilot was the Piccolo II by Cloud Cap Technology. This decision was based on reliability and ease of compatibility with other small UAS systems that our team has worked with in the past (i.e., Lockheed Martin Corporation and Raytheon Company). Following that decision, many items were purchased, including a pitot/static tube for air data collection, vibration mount for the Piccolo II, deadman/tachometer board for engine data collection and flight termination in case of system failure, servo wiring

harness, and an appropriate ignition system that could be interfaced with the deadman/tachometer board. Two Piccolo II autopilot units were purchased, so that one could be installed in the aircraft and the other could be used for lab testing. The second unit also served as a spare in case the other failed. A CCD camera with transmitter and antenna was purchased for forward-looking capabilities. Additionally, there were five antennas mounted on the aircraft to be used for payload configuration, autopilot communications, and GPS navigation. The autopilot, forward-looking camera, and payloads are all powered by Lithium Polymer (LiPo) batteries, with the aircraft's servos and ignition being powered by NiCad batteries. To ensure safe operation of the entire system, two sets of batteries were purchased and are kept charged at all times. Before and after each flight, the health of all batteries are checked to guarantee successful and safe flights, and if need be, the batteries are replaced. Furthermore, the autopilot can constantly monitor the voltage of the autopilot and servo batteries from the autopilot console.

After collection of the critical components, the next step in operation was to become familiar with the Piccolo II autopilot system, which was done by studying the available Piccolo II documentation that came in the autopilot package. In the documentation, an outline of the integration process could be found. The documentation provided does not lead the user step-by-step through the integration process, but rather helps direct the user along the correct path, because the integration process is system-specific, and it would be virtually impossible to have installation instructions that would work for every UAS platform.

One of the initial steps Cloud Cap Technology recommends is the development of a computer model of the aircraft so that it can be flown in the Piccolo II simulation. This model then becomes a link between simulation and actual flight. This particular step, often omitted by others, was strongly emphasized, and requires a model of the aircraft to be developed as accurately as possible. This model requires the dimensional measurements of the control surfaces, wings, tail section, fuselage, landing gear location, and the location of the center of gravity (CG). An accurate measurement of the location of the CG is critical, as most measurements are in reference to the CG location.

After the detailed physical information of the aircraft was collected and recorded, a computer model of the aircraft was created using a program called AVL, supplied by Cloud Cap Technology in the software package. AVL runs a virtual wind tunnel over the model and develops its aerodynamic coefficients that are later used by the autopilot to control the aircraft, as shown in Figure 32. After the simulation is run, the aerodynamic coefficients are saved in an XML file generated by AVL. The next step was to create a lookup table (LUT) for the propeller and the engine. To create the LUT for the propeller, two other programs supplied by Cloud Cap Technology, Prop.exe and JavaProp.exe, were used. The necessary parameters required for input are the pitch and diameter of the propeller, expected RPM, spinner or propeller hub diameter, and design airspeed. The programs create an LUT containing thrust and torque data for the propeller based on the RPM and forward speed of the aircraft. Next, the simulator calculates the advanced ratio, and based on the LUT, determines the coefficient of thrust and coefficient of power that are used to calculate the thrust of the propeller.



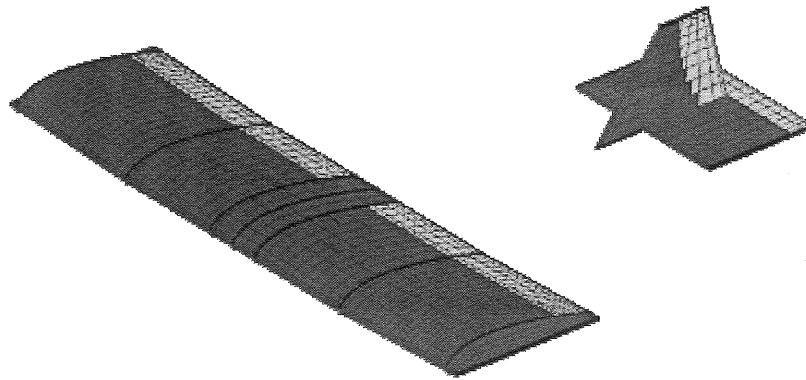


Figure 32: Screenshot from the AVL program.

The data required for the engine LUT was not provided by the manufacturer, causing this table to be more of a challenge to create. The required information for the table was the maximum horsepower, minimum and maximum RPM, and power output at specific RPMs. Since no information for the engine was available, an engine with similar specifications and data was found. Based on the data that was collected from the other engine, an estimate of our motor data was extrapolated into an LUT. Finally, the information from the XML file, and the propeller and engine LUTs along with the aircraft weight, CG location, and landing gear location were compiled into a .txt file, which were used directly by the Piccolo II autopilot during both simulation and actual flight.

After the .txt file was created, flight simulations using the Piccolo II software were conducted. The content of the .txt file for Super Hauler is included in APPENDIX F. In simulation mode, aircraft behavior was able to be tested as if it was in actual flight.

If the model in the simulation did not perform as expected, necessary corrections were made to the autopilot gains without the need for field testing the aircraft and possibly risking damage. The external pilot for operations was able to take manual control while in simulation and fly the model around to see if it responded and behaved properly. After a few iterations of gain adjustments, the simulation model flew to the liking of the external pilot and was cleared for actual flight. The gain settings in Piccolo Command Center are shown in APPENDIX G. The benefits of this simulation cannot be emphasized enough, since it allowed the pilots to see and feel how the aircraft would perform, in the safety of a lab environment and without even starting the engine. The performance of the aircraft in simulation is directly related to the accuracy of the model and measurements. Since such precise measurements were taken and no steps were skipped, the team was quite confident that the aircraft would perform the way it should when the autopilot was turned on for the first time during actual flight.

#### 4.3.2 Hardware integration

Hardware integration into the airframe incorporated many different challenges into our work. Integration of the Piccolo II autopilot system, deadman/tachometer board, and servo harness provided difficulties with electromagnetic interference (EMI) concerns requiring different methods of shielding to be included in the integration of the components. EMI issues occurred throughout the integration process and were dealt with in the best manner possible. The main concern was that EMI would cause the servos to operate incorrectly during flight, resulting in damage to the aircraft. Copper tape was used to cover all of the servos and to make ground planes for the antennas that were

causing noise in the system, as shown in Figure 33. Upon completion of the shielding, the servos operated much better, and we were confident that operations would be successful.

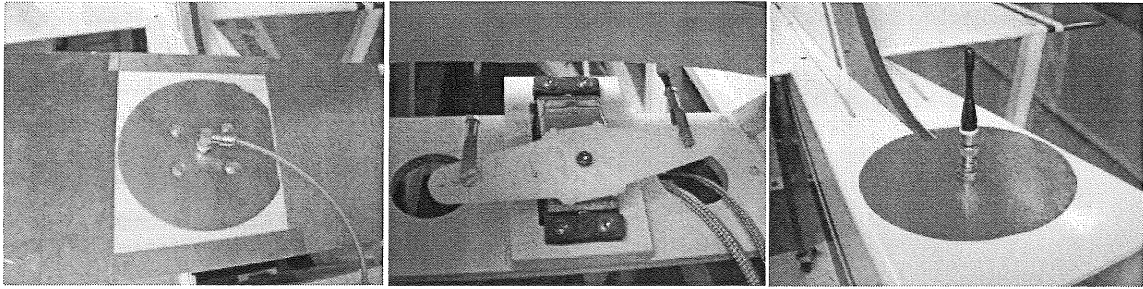


Figure 33: Copper plate shielding and antenna ground plates.

Many of the wires that ran on the inside of the aircraft, including all the servo and ignition cables, were rewired and shielded with an EMI safe casing, as shown in Figure 34. Servo “chatter” due to electromagnetic interference was something that was studied for many hours and never completely solved. Even with the precautions that were taken, there was still a residual amount of chatter in the servos.

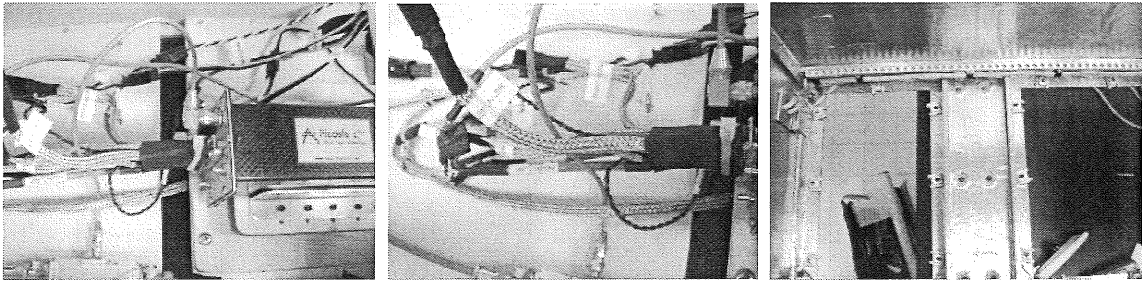


Figure 34: Servo harness and ignition wire shielding.

With the primary research on campus being payload development, it was important for the aircraft to perform in the same way for any payloads installed in the aircraft. The autopilot is mounted directly behind the payload bay, so there was some

initial concern regarding EMI between the payload and the autopilot. The payload bay was heavily modified by lining the entire bay with copper tape and placing aluminum plates on the front and back walls. All wires coming into the bay were shielded and passed through a small hole lined with EMI gasketing, as shown in Figure 35.

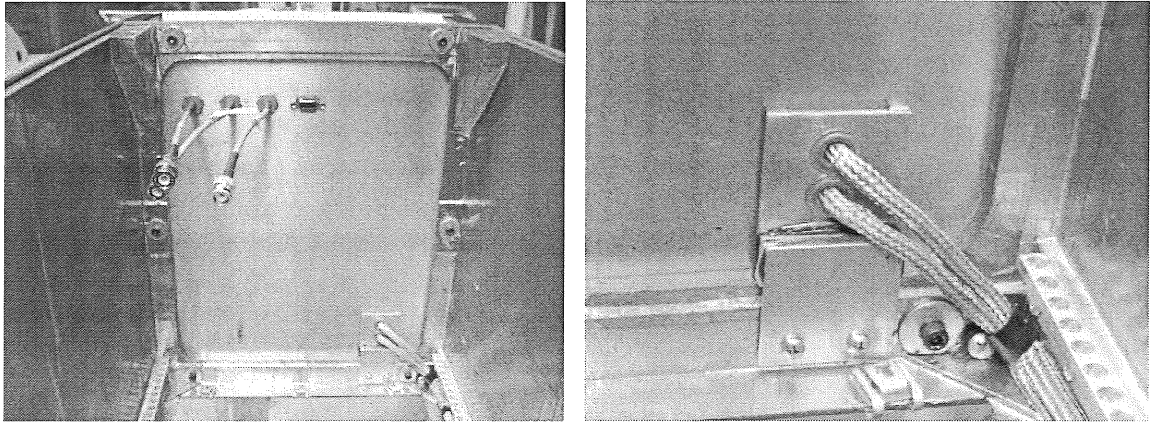


Figure 35: Payload bay and aluminum firewall with EMI shielded pass-through hole.

These precaution steps ensured safe and interference-free operation of both the aircraft and the payloads. The benefits and advantages gained from the process of autopilot integration into the UAV cannot be emphasized enough and were kept in mind throughout the development of the system. We truly believed that this complicated course of action was superior to the alternative of acquiring a UAV with an autopilot system already installed. During the integration process, we were able to become more familiar with the autopilot itself, including its design and capabilities, such as post flight data analysis, to gain a better understanding of the UAS system as a whole. Another crucial point is that the payloads are an integrated part of the UAS, and they can directly interface with the autopilot. This operation requires not only knowledge of the autopilot operation and interface procedures, but also demands modification of the aircraft itself.

## CHAPTER 5

### TESTING

Testing of the system is an ongoing process that plays a crucial role in the performance and reliability of the project. Quite often, as in the case of ELVIS, the system is so complex that it is necessary to break it into smaller subsystems and then test each subsystem individually. This type of approach is highly desired in order to more easily and more accurately identify problems and imperfections in the system. Data gained from each subsystem can be effectively used to fine tune that subsystem and improve overall system performance. In addition, it allows us to better understand and predict the behavior of the system.

#### 5.1 Preliminary component tests

Testing was divided into smaller subsystem tests in order to more easily identify any problems at the lower level. Once each of the subsystems was successfully tested, they were assembled into a full system test, and series of UAS flight tests were performed as well.

##### 5.1.1 Laser transmitter

The original laser TX came with a 5mW red laser at 660nm. In order to achieve successful communications over longer distances, four more powerful options were

explored: a 50mW laser at 660nm wavelength, a 100mW laser at 660nm, a 150mW laser at 808nm, and a 200mW laser at 808nm. The most significant limitation that we have faced during testing was the ability of the laser diode driving circuit to supply enough current to drive the diode without saturating the modulation transistor. If transistor saturation occurs, the laser light cannot be correctly modulated, and thus no video signal can be reconstructed at the receiver. The tests performed with the diodes mentioned previously are listed in Table 2. The recommendations for the laser system are presented in Section 6.2 of this thesis.

Table 2: Laser diode tests.

Laser Diode Measurements							
Diode Rating (mw)	Laser Wavelength (nm)	Actual Power (mW)	Q1 C-E Voltage(V) (1.1-1.35)	R11 Value (Ohms)	R11 Current (mA)	Video transmission results	Comments
50	660	31.51	1.19	24	104.39	In all the cases the video did not drop, but the quality of it varied. The tests were performed keeping the voltage across Q1 within its limits, so that it was not getting saturated.	
		26.58	1.35	24	98.67		
		27.95	1.30	24	100.25		
		29.59	1.25	24	102.08		
		30.68	1.20	24	103.69		
		32.05	1.15	24	105.49		
100	660	33.70	1.10	24	107.46	drop out	Tests performed without optics, over a distance of 2-3 feet. Laser spot covering almost entire receiver
		31.51	1.43	24	92.50	still there, sensitive to AOI	
		33.15	1.44	24	97.50	good	
		42.74	1.18	24	102.08	still there	
		50.96	0.82	24	114.58	still there, bad quality	
		57.88	0.77	24	116.25	drop out	
150	808	41.10	0.81	27	103.70	good	
		120.55	2.34	24	107.08	a lot of static with some video	
		81.64	1.40	33	87.27	a lot of static with some color video	
		68.49	1.59	33	81.52	a lot of static with some color video	
		57.26	1.10	43	74.19	no video	
		98.63	1.70	27	94.44	color video w/static noise	
200	808	124.11	1.39	27	105.56	color video w/slanted line noise	Test performed about foot away with the bandpass filter installed.
		267.12	1.47	27	102.22	color video w/slanted line noise	
		168.77	1.44	24	123.33	drop out	
		159.73	1.53	24	119.17	good	
		158.63	1.56	24	118.75	good, but flickery a bit	
		153.97	1.61	24	117.50	unstable video	

The tests were performed in the lab at distances of about two-to-four feet and without the laser beam expander. The actual power reading was taken right at the output

of the laser diode using our optical power meter. The trick to capturing an accurate reading was to have the laser beam focused as accurately as possible at the point of measurement, because the input to the optical aperture of the power meter is about 4mm in diameter. By manipulating the value of the R11 resistor on the laser TX board, we were trying to find the most optimal potentiometer setting. The current through R11 and the voltage across the Q1 transistor on the laser TX board was changing due to adjustment of the potentiometer. In this case an R11 resistor is used for course adjustment and the potentiometer is used for fine adjustment. Components R11 and Q1 are shown in Figure 36.

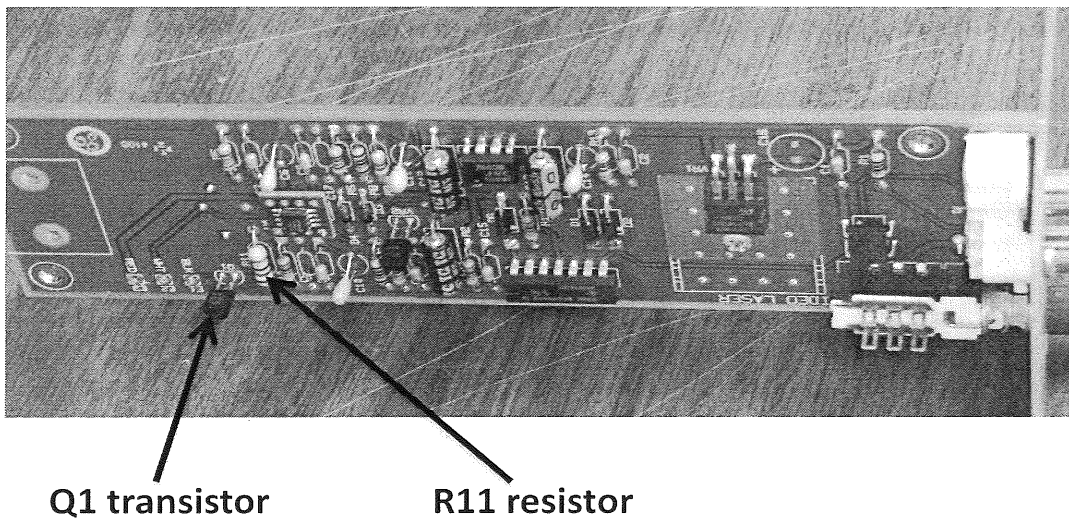


Figure 36: Laser TX board with R11 and Q1 annotated.

### 5.1.2 Laser receiver

The laser RX testing was performed in parallel with the laser TX, simply because you cannot really test one without the other. The design and modifications of the original RX are described in detail in Section 2.2 of this thesis. The RX board contains one

potentiometer to adjust sensitivity of the receiver. That potentiometer was set in an optimal position to ensure correct operation of the receiver and the best video quality possible. The potentiometer was set in the preliminary stage of testing, when the new photodiode array was installed, and was not adjusted much, if at all, throughout the testing of the different laser diodes. This might have not been the most optimal way of testing, but from what we have seen, adjusting the potentiometer on the RX board was not that effective in improving video quality.

### 5.1.3 Bandpass filter

The current bandpass filter has been tested on a few different occasions in different environments. The filter is a 6cm x 6cm bandpass filter with center wavelength 808nm, a maximum angle of incidence (AOI) of 35degrees; a bandwidth of 70nm, and a typical center wavelength transmission of 85% as shown in Figure 5. According to the test results obtained from the actual filter by the manufacturer, at 0degree AOI the transmission is 86%, and at 30degrees AOI the transmission is 94%. Additional tests were performed in the lab with a flashlight shining onto the receiver along with a transmitted video signal. Without the filter, the receiver photodiode array became saturated, and the received video signal would get dropped. With the filter installed, the video would continue to be displayed while the flashlight was incident on the receiver. A series of short tests were also performed outside in sunny conditions. Without the filter, video transmission could not be established. Again, installing the filter on the receiver, this enabled signal transmission, but the quality of the video was still affected. Blocking the direct sunlight with an object improved the quality of the signal significantly.



#### 5.1.4 Onboard computer

The current PC 104+ onboard computer was equipped with an eight serial port extension board. Four of those ports are currently utilized, and to do this, custom cabling was required. Four DB-9 cables were made, with one interface connector that plugs into the computer as described in Section 3.1. To verify the connectivity of those cables and the functionality of the serial extension board, a test was set up between the onboard computer and a notebook computer using Hyper-Terminal in the Windows environment. By simply sending a text message from one computer to the other and vice versa, duplex communications was tested. The criterion for passing the test was to see the message sent from one platform appearing on the screen of the second platform. Each of the four serial ports was tested separately. The pass-fail results are shown in Table 3. In similar fashion, the serial ports were tested in the Linux environment. Text strings were sent from the serial monitoring software in the Linux environment to Hyper-Terminal on the Windows platform and vice versa.

Table 3. Pass-fail results for serial communications.

PLATFORM	MESSAGE SENT	MESSAGE RECEIVED	RESULT
Notebook PC	YES	N/A	PASS
Onboard PC	N/A	YES	
Notebook PC	YES	N/A	FAIL
Onboard PC	N/A	NO	
Onboard PC	YES	N/A	PASS
Notebook PC	N/A	YES	
Onboard PC	YES	N/A	FAIL
Notebook PC	N/A	NO	

### 5.1.5 Position sensing diode (PSD)

Recently, a PSD was purchased in order to evaluate its potential use in the ELVIS project. The Pacific-Silicon Sensor PSD consists of two parallel 10mm x 10mm photodiodes, one for the x-direction measurement and one for the y-direction measurement, and an amplifier PCB for the analog voltage position outputs. We chose to try a PSD based on the fact that they are widely used among laser guided weapons for tracking a laser designated or “painted” target. The idea is if we can place a light beacon at our receiver location and mount the PSD on the gimbal next to the laser transmitter, we should be able to “lock on” and track the receiver with the PSD’s position feedback. In order to have a better understanding of the PSD functionality, many initial tests must be conducted. Table 4 shows some of the preliminary tests that were concluded to characterize the PSD.

Table 4. PSD tests and associated pass-fail criteria.

PSD Tests	What is tested	Pass	Fail
Analog output range	The manufacturer specified output range is $\pm 12V$ based on a $\pm 15V$ supply.	Output range is greater than $\pm 11V$ .	Output range is less than $\pm 11V$ .
Analog output linearity	The manufacturer specified linearity of the outputs is no less than 99% of the full scale output.	Output linearity is greater than 95% of full scale.	Output linearity is less than 95% of full scale.
Range of detection	Characterize the minimum incident light power on the PSD for a continuous output reading.	No Pass/Fail Criteria.	

The first two tests listed in Table 4 are based on the manufacturer's specifications from the PSD data sheet. Our pass-fail criteria, however, are a little more relaxed, since we are interfacing with an imperfect PIC microcontroller system and output scaling circuitry. The PSD scaling circuit designed in Multisim is shown in Figure 37.

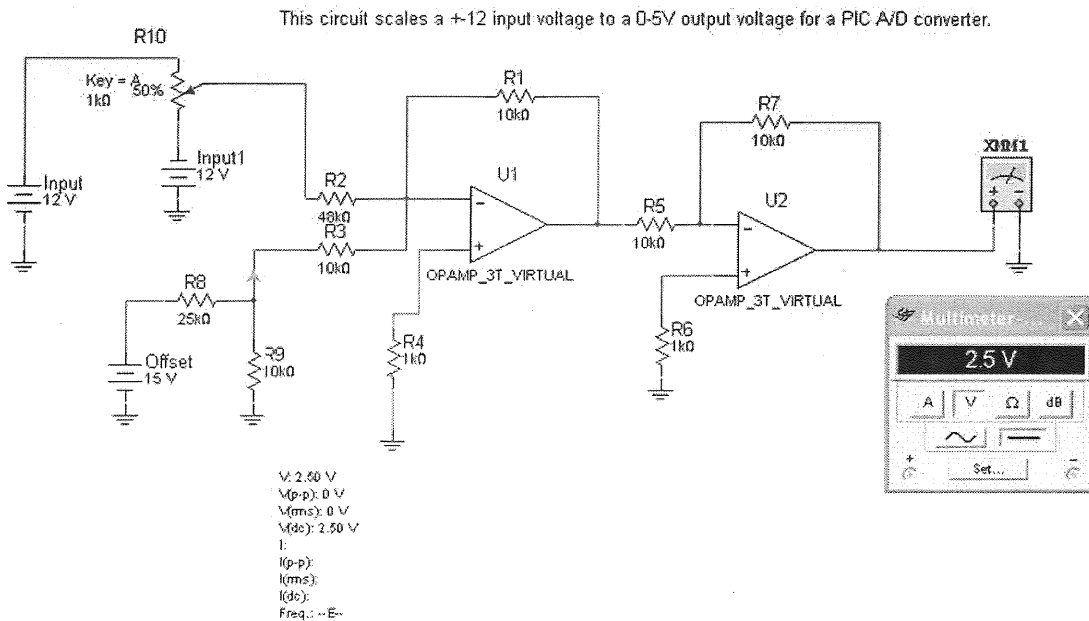


Figure 37: PSD scaling circuit.

The third test listed in Table 4 does not have any pass-fail criteria. This is because the minimum light spot detection power is not specified by the manufacturer. This test, however, is critical for our application. We need to know at what minimum light intensity the PSD will give us an accurate output position reading. This will help us to identify how powerful of a beacon we need or if any sort of optics in front of the PSD are required to achieve the desired detection range. In addition, these tests need to be

performed with and without a near infrared bandpass filter in front of the PSD to further characterize the behavior of the system. Figure 38 shows the initial test setup to evaluate some of the PSD parameters.

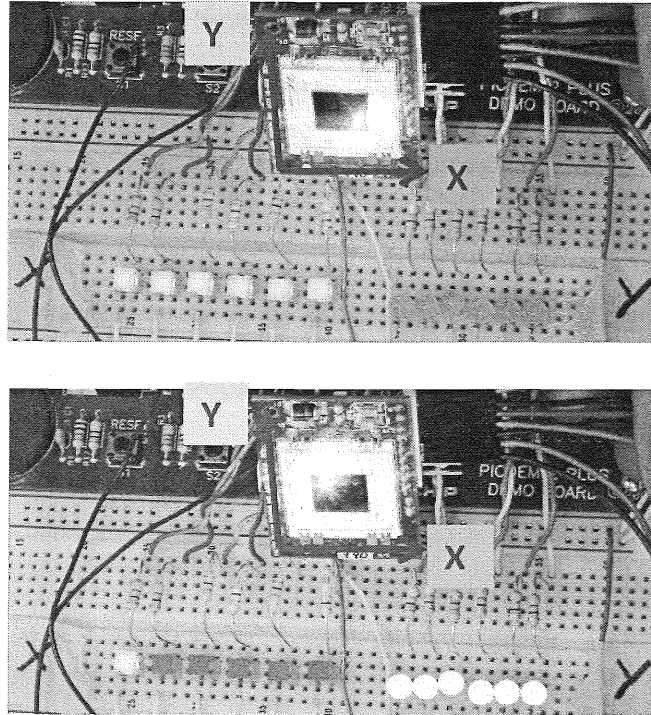


Figure 38: PSD testing.

In Figure 38, a green laser light was incident on the PSD. The green and yellow LED's light up with respect to the position of the green laser spot on the PSD. The top picture in Figure 38 shows the spot at the far end of the x-axis of the PSD and at the bottom of the y-axis, and the LED's verify that position. The bottom picture shows the opposite. The laser spot is simulating a focused light spot that would represent a laser beacon aimed at our receiver. The PSD can sense where this beacon is at in its field of view, so commands can be sent to the gimbal to compensate for any pointing error. More research needs to be done in order to select the correct optics to focus the beacon onto the PSD.

### 5.1.6 Joystick software test

Custom software for controlling the gimbal through the joystick was developed in MATLAB. Two separate scripts are used: one for the ground-based computer, and the other for the onboard computer as described in Section 3.5. The test for both of the codes was performed in two steps. First, the code was tested using a wired serial connection between two computers without the autopilot communications link. The second step was to actually use the autopilot communications link to send the commands and verify communication. The pass-fail criteria for both of these tests were the same. The goal was to send the command, successfully split it, and observe the operation of the gimbal and camera working at the same time. Table 5 presents pass-fail results for the software tests.

Table 5. Pass-fail results table for joystick software.

	WHAT IS TESTED	PASS	FAIL
<b>JOYSTICK SOFTWARE</b>	Sending commands from ground-based computer.	Command was sent.	Command was not sent.
	Splitting the code from the ground based computer.	Command was split in two separate commands and sent to different com ports.	Command was not split or only one command was sent.
	Simultaneous operation of gimbal and camera.	Gimbal and camera can be controlled simultaneously.	Only one device is responding to the commands.
	Synchrony of the gimbal.	Gimbal maintains synchrony throughout the test.	Gimbal goes out of synchrony at any point of the test.

### 5.1.7 Gimbal optimization

One of the major problems that we have faced during our first flight tests and later on during the incorporation of gimbal joystick control was the synchrony of the gimbal. In short, the internal settings of the gimbal, such as starting velocity and maximum velocity, were causing the system to lose its orientation, eventually leading to crash. Therefore, a test was constructed to isolate the parameter or parameters that were causing misbehavior of the system. The procedure consisted of changing only one setting and monitoring the behavior of the gimbal. After nearly 40 trial and error tests, we tuned the system to successfully maintain constant operation without losing synchrony. The partial results of the tests are shown in Table 6.

Table 6. Gimbal optimization test table (split in half).

Parameter	Pan Base Speed	Tilt Base Speed	Pan Accel	Tilt Accel	Pan Max Vel	Tilt Max Vel
Command	PB	TB	PA	TA	PU	TU
Baseline	500	500	6000	6000	4002	4002
Trial 17	2000	2000	6000	6000	3500	3500
Trial 38	2200	2200	6000	6000	3300	3300

PMH	TMH	PHR	THR	Tilt Disabled	Pwr Source	Delay (ms)	Comments	Out of Sync
PMH	TMH	PHR	THR	na	na	na	na	na
y	y	y	y	n	ac	250	not good at higher speeds	y
y	y	y	y	n	ac	100	not good	pan-y,tilt-n
y	y	y	y	n	dc-28.2V	100	good	n

The table is divided in half, and what is shown here are two sections that are read left-to-right as one piece. The very top row in both sections corresponds to a parameter that was varied or manipulated during the tests. It should be mentioned that PMH and TMH represent high power mode for the pan and tilt motors, respectively. Also, PHR and THR represent regular hold power mode for the pan and tilt motors, respectively. The next two rows correspond to commands sent to the gimbal and baseline set up, respectively. We based all of our measurements and changes on the baseline parameters. The remaining two rows correspond to trials 17 and 38, respectively. The fields in red contributed to the out-of-synchrony gimbal operation in the corresponding trail. Based on the tests performed with the gimbal so far, there are a few items that we would recommend. They will be discussed in Section 6.4 of this thesis.

## 5.2 System tests

After all of the individual subsystems have been characterized and tested, a full system test is necessary to make sure that the subsystems interact with one another in a predictable manor. The way we do this is to perform ground testing using a truck which holds the aircraft with the ELVIS payload installed in it. While the truck is driving around, the ELVIS payload will either be running the tracking algorithm to track the stationary receiver, or it will be controlled manually with a joystick in an attempt to aim the laser transmitter at the receiver. This type of test is as close as we can get to an actual flight test, and provides a great deal of useful information about the system as a whole

and how the subsystems interact with each other. Figure 39 shows the aircraft track mount, and Figure 40 shows how the whole system is set up for the truck test.

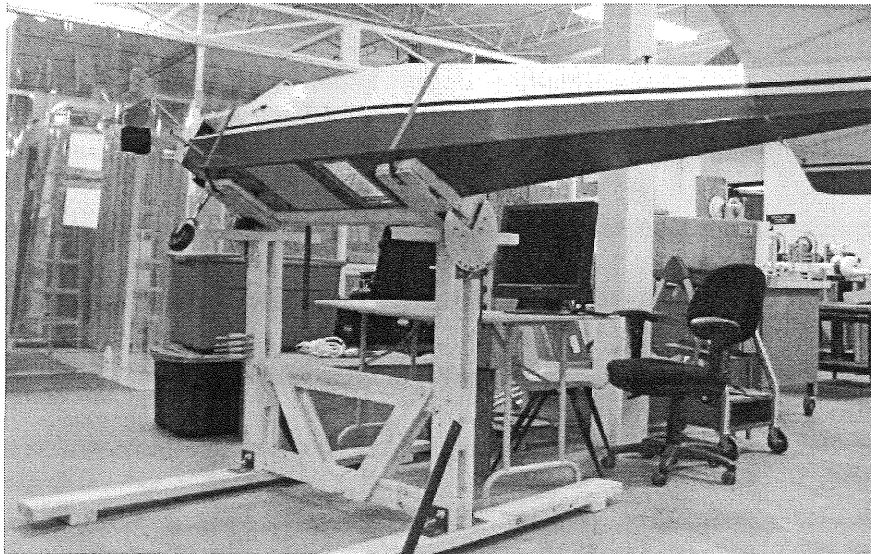


Figure 39: Aircraft truck mount.

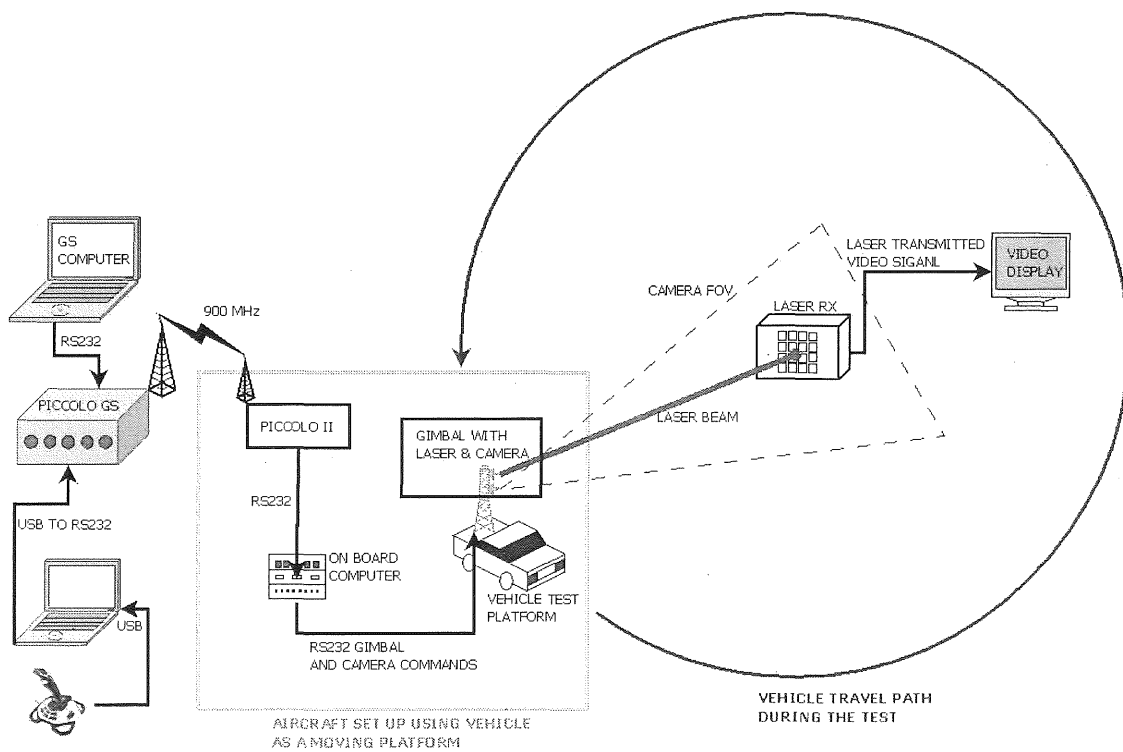


Figure 40: Truck test setup.



### 5.3 Simulations

The two-axis tracking algorithm was tested in the Embedded MATLAB environment before the flight tests occurred. Piccolo Command Center (PCC) was adopted to act as the onboard Piccolo II autopilot system. In the PCC interface, a series of flight paths were created to test the two-axis gimbal motion limitations by varying the shape of the path, flight altitude, and distance between transmitter and receiver. During the simulation, PCC sends the telemetry files of the simulated flight to the gimbal control function via RS232 serial communications. According to the location and motion information of the airplane provided, the gimbal control function calculates the angles for the pan and tilt unit. Figure 41 demonstrates the results from a square shaped flight path. According to the outcomes of the pan and tilt angles, the position where the line-of-sight vector intercepts the receiver location is calculated. The pointing error, the difference between the interception point and the GPS location receiver, was less than 1 millimeter. This theoretical error level verified the effectiveness of the serial communications function and the tracking algorithm. However, the simulated tests were in ideal conditions, which meant no vibration was introduced to affect the results. Due to the position control of the gimbal system, the jittering motion of the gimbal produces additional error during the flight tests.

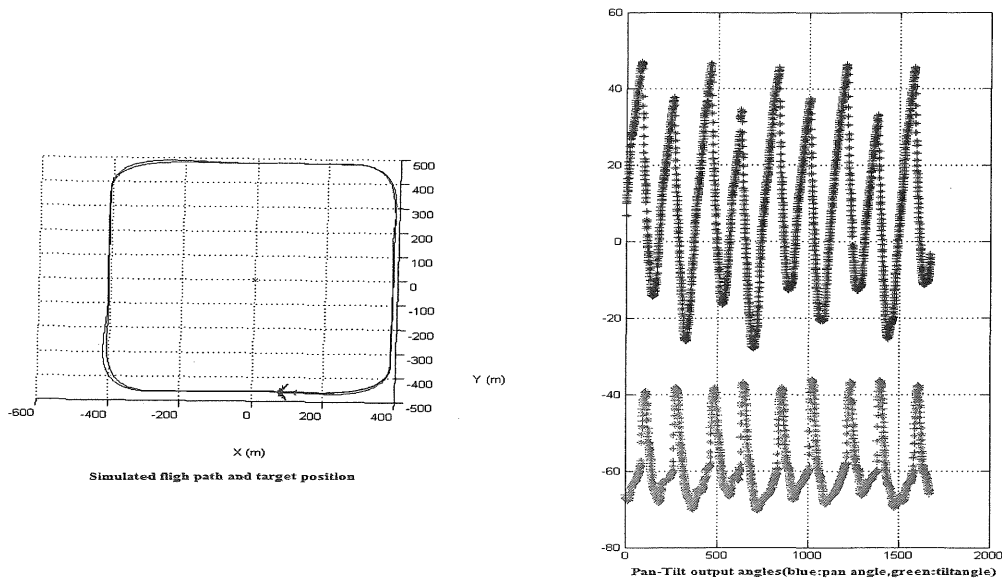


Figure 41: Simulation results for a square flight plan.

#### 5.4 Flight tests

As mentioned previously, three flight tests have been performed with the ELVIS payload in the Super Hauler UAS platform. The first flight test occurred on July 28-30, 2009, the second flight test on October 3- 4, 2009, and the third flight test took place on June 2-4, 2010. Each test was approximately twenty minutes in duration, and each was performed with a slightly different goal in mind. The purpose of the first trial was to test the GPS pointing algorithm during an actual flight and to determine whether or not a successful laser link could be achieved. The autopilot flight path for the test was carefully planned in order to obtain the highest probability for the gimbal to point at the receiving target. After a successful system test on the ground, the aircraft was sent to the predetermined flight path. With the UAS in the air, we could see exactly where the gimbal was pointing, since we had an RF video feed from the camera mounted on the

gimbal. This camera also has a controllable zoom that was used during the flight in order to obtain more precise information on where the gimbal was actually pointing. The RF video feed as well as the video signal from the laser receiver were both recorded in order to be analyzed later. Upon reviewing the laser receiver video, it was concluded that a laser link was never established with the UAS, since there was never a signal received by the ground station. This was likely due to a number of factors. The most obvious rationale is the fact that the GPS tracking was not performing as well as expected. This was deduced by examining the RF video feed. It seemed like the gimbal was slightly behind where it should have been when tracking the target. This reveals the potential need for a predictive algorithm to be implemented. Another likely explanation for not establishing a link is that the photodiode receiver was saturated from the ambient sunlight. This is why a bandpass filter is now being integrated in front of the photodiode array. Figure 42 shows a couple of snapshots from the RF video feed during the flight test. Each picture is from a different pass over the receiver, and they are at different zoom levels as well. The object in the middle of the circle in the pictures is the laser receiver. The receiver is sitting in the middle of a 12ft  $\times$  10ft tarp.

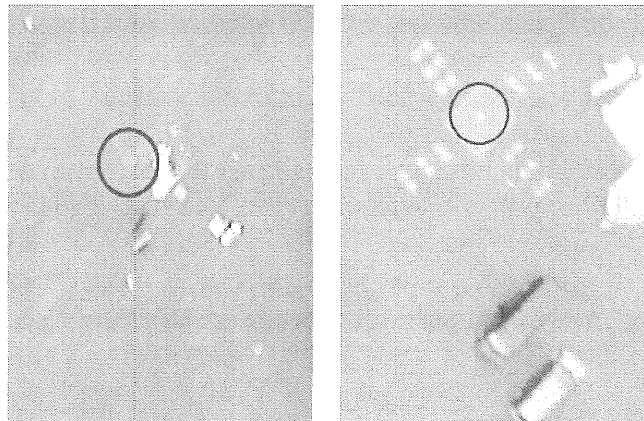


Figure 42: Snapshot from the RF video feed during the first flight test, July 28-30, 2009.

The second flight test was performed with a few minor modifications to the laser receiver. Eight ultra-bright wide angle near IR LED's were mounted around the photodiode array, as shown in Figure 1. This configuration was constructed to determine if they could be observed by the camera with the near infrared filter turned on. This was a test to see how effective this configuration would be for aiding in a machine vision-based fine resolution tracking system. Also, it should be mentioned that no changes were made to the GPS tracking algorithm due to time constraints. This time, the system test on the ground showed that the flight computer was not receiving GPS and IMU data updates faster than once per second, and after trying to resolve this issue without success, we decided to perform the flight test anyway. We conducted one short flight with the slow GPS tracking on and one with the gimbal fixed pointing down with a modified flight path to compensate. Again, the RF video feed as well as the laser receiver video output were recorded. After analysis, it was concluded that a link was never established between the laser transmitter and receiver, and it was found that the infrared LED's were not as effective as we had anticipated.

The third flight test took place almost ten months later. There were several changes made in order to improve operations of the system based on information and experience we gained from the first two flights. The main changes are provided as follows:

- The gimbal was optimized in order to eliminate out-of-synchrony operation.

- Gimbal and computer battery voltage was increased from 20.5V (fully charged), to 29.2V (fully charged) for more powerful, robust operation, and extended operation.
- The onboard computer was equipped with larger solid state hard drive and the operating system (OS) was limited exclusively to the Gentoo Linux OS.
- Four additional serial ports were added to the onboard computer for straightforward, reliable serial communications.
- Gimbal and SONY camera joystick control was added for enhanced manual control, tracking, and system debugging.
- Significant testing was performed to tune the laser TX board, in order to accommodate a more powerful laser diode at 808nm, unfortunately without greater success.
- The tracking algorithm was refined and debugged to eliminate known software glitches and also to speed up operation of the numerical algorithm.
- PSD technology for machine vision-based tracking was explored, but it has not yet been implemented into the system, since more research is required in this area.

The objective of the third flight test was to mostly focus on the improvements that were made with regard to the tracking algorithm and gimbal performance. We knew that video transmission would be almost impossible, simply because we were not able to successfully integrate the new laser diode into the system. We also did not have an appropriate bandpass filter for the 660nm laser wavelength, and from the test performed with the filter at 808nm, we proved that ambient light greatly influences video transmission. Therefore, the crucial point was to have 1.7GHz video transmission

working for the SONY block camera, so that we could verify the tracking performance of the gimbal and algorithm. Preflight bench tests at the field confirmed the correct algorithm operation and fast data update rates. Upon installing the payload inside the Super Hauler payload bay, we had troubles communicating with the SONY block camera via its serial port. Without serial communications, we could not zoom in or out or use the near IR filter, and therefore it would have been very difficult to determine tracking accuracy. Upon about half-an-hour of inspection and troubleshooting, we finally established the necessary communications and were ready for the flight. At that point the gimbal was still receiving telemetry data at 20Hz, so it was updating its position fairly fast. Once in the air, as long as the target was within the field of view of the gimbal dictated by its rotational limits, the tracking algorithm did a really good job of tracking the target on the ground. Unfortunately, due to the autopilot malfunctioning, we were forced to land prematurely. We also did not get a chance to test the joystick gimbal control in-flight, simply because the MATLAB code that runs on the ground-based computer was crashing. After several minutes of troubleshooting, we gave up the flight and allowed others to fly and test their payloads. It turned out that the MATLAB script we were trying to run was an old version. About five minutes after we gave up the flight, we ran the updated script and everything worked fine. We did not get another chance to fly the ELVIS payload during the June 2-4, 2010 flight days. Overall, we were pleased with the results of the last flight test. The knowledge gained from all three flights will serve as a base for the second generation of the ELVIS payload, and lessons learned will be kept in mind throughout the process of redesigning the payload.

## CHAPTER 6

### SUMMARY AND FUTURE RECOMMENDATIONS

While we believe we that have accomplished a great deal on the ELVIS project, there are still an abundance of items that need to be addressed to make this project more successful. This chapter will provide recommendations and serve as a basis for the future work in order to make the second generation ELVIS payload more reliable, robust, and successful in achieving air-to-ground laser communications.

#### 6.1 Machine vision-based tracking

In order to achieve the level of accuracy needed for pointing the laser transmitter at the receiver, a tracking method must be developed to augment the current GPS and IMU-based algorithm. An integrated machine vision-based tracking system has the potential to fulfill this need. As mentioned before, a PSD was tested to provide this functionality to the system. There is, however, a great deal of work that needs to be done to get this successfully integrated into the system. The basic idea is that the GPS and IMU-based tracking algorithm would be used for course-resolution tracking, in order to get the receiver into the field-of-view of the PSD, and then machine vision fine-resolution tracking would take over the control of the gimbal until for some reason the receiver exits the PSD's field-of-view. This type of hybrid tracking should be very efficient, and will provide redundancy should the UAS ever enter a GPS-denied environment for a short

period of time. In order to implement the PSD into the system, a near infrared beacon is needed on the ground-based target. The PSD would be mounted on the gimbal, and it would look for that beacon light on the ground. To further improve the robustness of machine vision-based tracking, a bandpass filter at the beacon wavelength should be installed in front of the PSD. The filter would also ensure that there would be no false tracking of any other light source but the beacon. Based on the position of the beacon light spot within the field-of-view of the PSD, position commands can be sent to the gimbal in order to maintain the beacon light source in the center of the field-of-view of the PSD, therefore looking at the target.

## 6.2 Laser modulation

After retrofitting the original laser TX with a new, more powerful laser diode in the near IR spectrum, we faced a problem with the TX board being capable of modulating the more powerful laser diode correctly. Some steps need to be taken to adjust the power distribution scheme so that the modulation will work correctly and therefore increase the transmitted video quality. The other, and probably preferred, possibility would be to purchase a new laser TX system that utilizes a digital modulation scheme such as amplitude shift keying (ASK), on-off keying (OOK), or code division multiple access (CDMA) in order to achieve a more robust, interference free transmission.

## 6.3 Receiver improvement

Another suggestion to improve the transmission range of the system is to add some sort of optics such as a Fresnel lens in front of the receiver photodiode array. This



would essentially add “gain” to the laser path, and therefore increase the achievable range. This will only be effective if the lens itself is larger than the photodiode array, and it will need to be focused properly so that the receiver is at the focal point of the lens. This will, however, add significant size to the receiver, and special considerations must be taken to ensure that the receiver is never pointed directly at the sun, as this would possibly damage the photodiode array even if there is a bandpass filter installed. In addition, adding the optics component would allow having a larger laser spot on the receiver and thus make pointing and tracking easier tasks. The second recommendation is to put the receiver and its optics onto a rotational gimbal that would track the aircraft at all times. This would ensure that the laser beam incidence angle at the receiver is 90degrees, which in turn would increase the effectiveness of the receiver and increase the range of laser transmission. Remember that the bandpass filters are effective only at the maximum angle of incidence. For example, the current bandpass filter has a maximum angle of incidence of 35degrees with respect to the normal to the photodiode array. Beyond that angle, the laser transmission is virtually entirely blocked.

#### 6.4 Gimbal improvements

The current gimbal system used on the ELVIS has rotational restrictions in the panning and tilting planes that significantly limit its tracking capabilities. Pan range is limited from  $-159^{\circ}$  to  $159^{\circ}$ , and the tilt range is limited from  $-47^{\circ}$  to  $31^{\circ}$ . Therefore, it will be beneficial, or even required, to either purchase or design and build a fast responding gimbal, with a high resolution,  $360^{\circ}$  pan rotation range, and  $180^{\circ}$  tilt rotation range. We believe that integrating this type of gimbal will significantly improve the tracking

capabilities of ELVIS by extending the range or field-of-view of the laser TX. Probably the most significant restrictions that are going to drive the design are the weight and the size of the payload unit. The aircraft can handle only up to 25lbs of payload. This 25lbs includes the gimbal, onboard computer, laser TX, camera, all electronics, and Lithium Polymer batteries. All this hardware adds up fairly quickly, so the weight budget must be kept in mind throughout the design process. The other design consideration is the size of the gimbal. The payload bay has dimensions of 22in  $\times$  11.5in  $\times$  13in (L $\times$ W $\times$ D), and all payload components must fit within that volume.

#### 6.5 Software refinement

First of all, the current GPS tracking algorithm needs to be refined to incorporate velocity control of the gimbal, in comparison to position control that is currently implemented. Velocity control will enable much smoother and seamless operation of the gimbal, making the pointing system more stable, robust, and reliable. After the GPS tracking algorithm is functioning as expected, the joystick control software should be merged into it to provide a flawless transition from automated control to manual joystick control and back. After the combined GPS and joystick software is tested and verified, the code developed for the machine vision-based tracking method needs to be inserted into the GPS/joystick code to provide a complete closed loop software solution for the system. The new software will then have the ability to provide course receiver tracking through the DGPS algorithm, fine precision adjustments through the machine vision-based algorithm, and finally manual pointing control through the joystick algorithm. To








even further improve the accuracy of the tracking algorithm, a Kalman filter or particle filtering algorithm should be investigated.

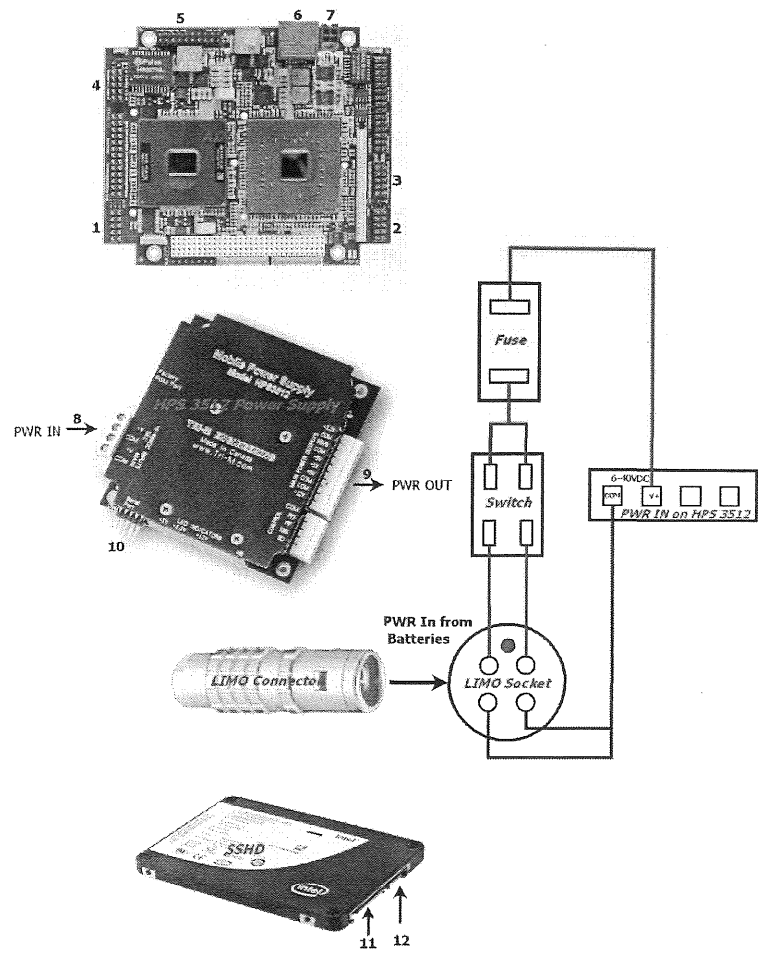
## 6.6 Conclusion

Even though lasers have been around for a long time, free space laser communications is a fairly new discipline still early in its development. Current systems used by NASA [25] and the military require a substantial amount of resources to operate and are very complex in design. The purpose of this design was to introduce a proof-of-concept of a low-cost air-to-ground laser communications system between a small UAS platform and a fixed ground control station. There is still a tremendous amount of work remaining to overcome major obstacles, but based on current successes and progress, we are confident that the system will become fully operational and extended to UAS-to-UAS free space laser communications.

# APPENDIX A

## Wiring diagram of PC 104+ components

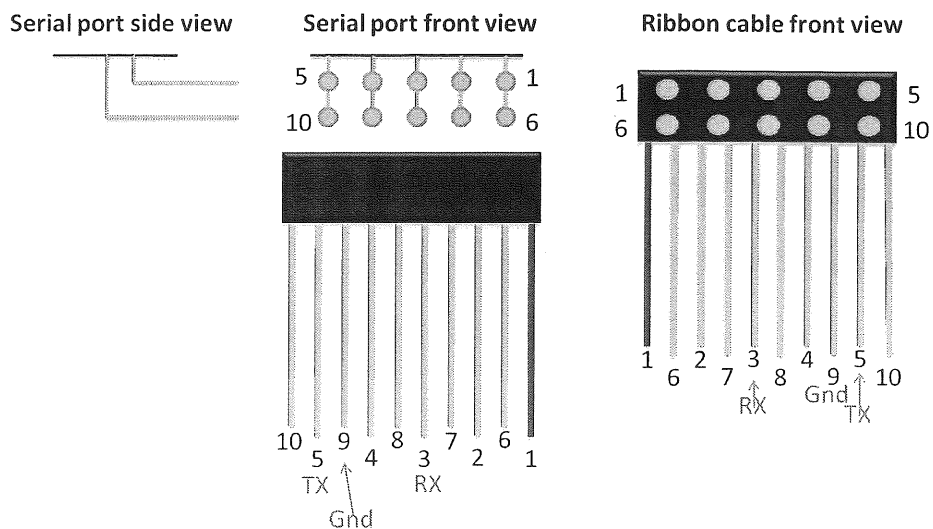
- Advanced Digital Logic (ADL) Cables Used**
- 1 
  - 2 
  - 3 
  - 4 
  - 5 
  - 6 
  - 7 
- 8 Main power input from battery
  - 9 Main power outputs to the ADL 945PC (5V), Patriot SSHD, and to the fans (12V)
  - 10 Serial port to connect to COM 2 on the ADL 945PC
  - 11 Power input to the SSHD (5V) from HPS 3512
  - 12 SATA cable input/output between SSHD and ADL 945PC



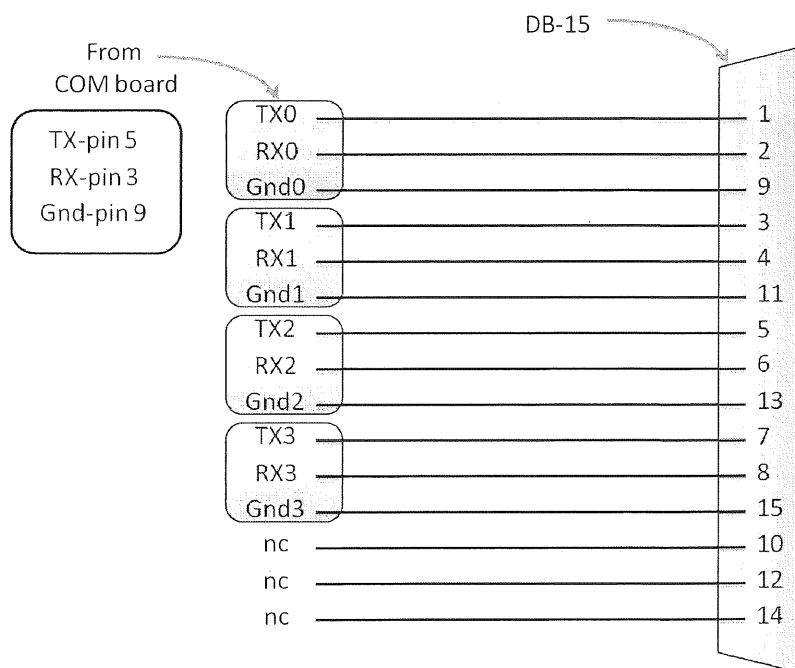
## APPENDIX B

### MSMX104+ serial port pin out

#### Serial expansion board output port pin out (8 ports available on the board)



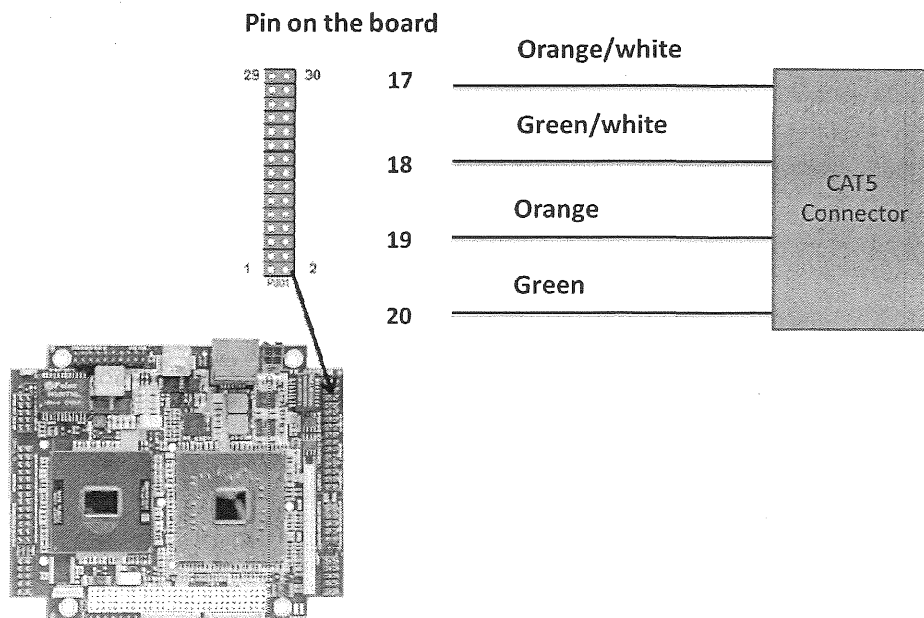
#### Wiring schematic from expansion board to DB-15



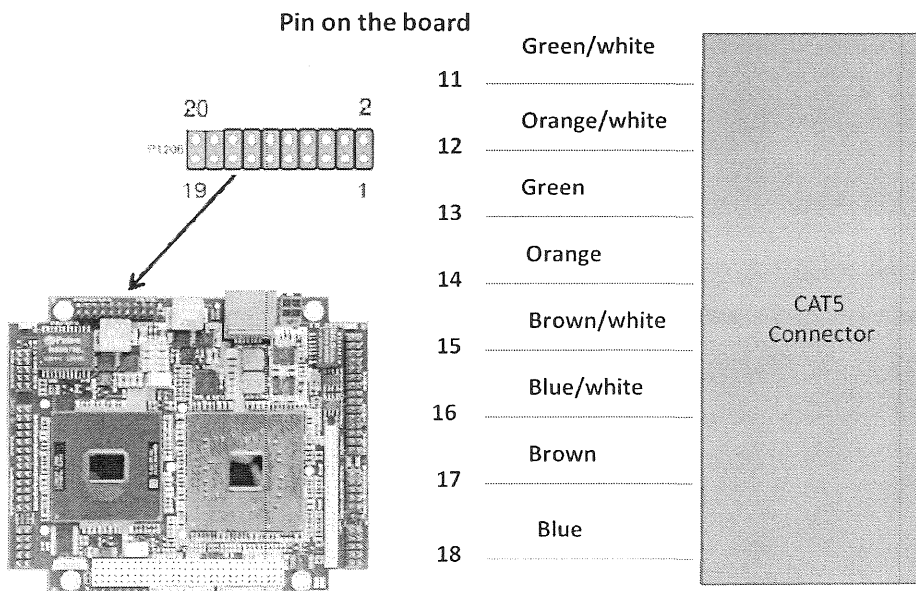
## APPENDIX C

### LAN 1 and LAN 2 internet connectors pin out

#### LAN 1 connection pin out



#### LAN 2 connection pin out



## APPENDIX D

### Ground-based computer MATLAB code for joystick control

```
%% Joystick Gimbal/Camera control
% Jason Blakely, Mario Czarnomski
% University of North Dakota
% 3-31-10

%Clear MATLAB workspace
clear all
close all
clc
pause on

%Preallocated arrays
pan=zeros(1,4);
tilt=zeros(1,4);

%Get user input for COM port number to use
COMport=streat('COM',(num2str(input('Enter COM port number to use: '))));

%Get user input for low speed sensitivity
indl=input('What low speed joystick sensitivity do you want(1= Low, 2= Medium, 3= High):
`);

if indl==1 || indl==2 || indl==3
    switch indl
        case 1
            indl=7;
        case 2
            indl=8;
        case 3
            indl=9;
    end
else
    indl=8;
end

%Setup joystick object
joy=vrjoystick(1);

%Set up serial COM port. Output buffer size of 22: 16 for joystick and 6 for camera
commands
com=serial(COMport,'Baudrate',9600,'Databits',8,'ByteOrder','bigEndian','outputbuffersize
',22);
fopen(com);

%Show figure with button functions
scrsz = get(0,'ScreenSize');
cx=scrsz(3)/6;
cy=scrsz(4)/8;

xs=scrsz(3)*2/3;
ys=scrsz(4)*3/4;
```

```

figure('un','pix','pos',[cx cy 85nclu],'menub','n','resize','of');
uicontrol('sty','fr','un','pix','pos',[15 15 xs-30 ys-30],'backg',[.1 .1 .9]);
uicontrol('sty','tex','un','pix','pos',[35 35 xs-68 ys-68],'backg',[.8 .8 .0],...
    'stri',{' ','ELVIS Joystick Control ','Jason Blakely & Mario Czarnomski', '4-
6-10',...
    'University of North Dakota','', 'Button Assignment: ',' ', ' Button 1
(Trigger): Zoom In',...
    ' Button 2 (Thumb): Zoom Out', ' Button 3: Digital Zoom Off'...
    , ' Button 5: Digital Zoom On', ' Button 4: IR Filter Off',...
    ' Button 6: IR Filter On', 'Button 7: Linear Input Scaling',...
    ' Button 8: Medium Exponential Scaling', ' Button 9: High Exponential
Scaling',...
    ' Button 12: Kill Switch!'],'fonts',14,...
    'fontname','Arial Black')
drawnow

%Initialize buttons variable for while loop
buttons = zeros(1,12);

%% Loop until button 12 is pushed
while buttons(12)==0;

%Read status of joystick commands
[axes, buttons] = read(joy);

%Test button 11 and send zero position command if pressed
if buttons(11)==1
%     fwrite(com,[116 73 10 48 48 48 48 48 48 48 48 48 48 48 48 129 1 4 7 0 255])
%     pause(.2)
%     fwrite(com,[116 73 10 48 48 48 48 48 48 48 48 48 48 48 48 129 1 4 7 0 255])
%     pause(.2)
%     fwrite(com,[116 73 10 48 48 48 48 48 48 48 48 48 48 48 48 129 1 4 7 0 255])
%     pause(.2)
%     fwrite(com,[116 73 10 48 48 48 48 48 48 48 48 48 48 48 48 129 1 4 7 0 255])
%     pause(.2)

    fwrite(com,[116 115 48 53 48 48 48 10 112 115 48 53 48 48 48 10 129 1 4 7 0 255]);
    fwrite(com,[116 115 48 53 48 48 48 10 112 115 48 53 48 48 48 10 129 1 4 7 0 255]);

%     fwrite(com,[116 112 48 48 48 48 48 10 112 112 48 48 48 48 48 10 129 1 4 7 0 255]);
%     pause(.2)
%     fwrite(com,[116 112 48 48 48 48 48 10 112 112 48 48 48 48 48 10 129 1 4 7 0 255]);
%     pause(.2)
%     fwrite(com,[116 112 48 48 48 48 48 10 112 112 48 48 48 48 48 10 129 1 4 7 0 255]);
%     pause(.2)
%     fwrite(com,[116 112 48 48 48 48 48 10 112 112 48 48 48 48 48 10 129 1 4 7 0 255]);
%     pause(5)

end
%% Joystick commands for gimbal
% Get x and y axes data points
x=axes(1);
y=axes(2);

%Test sign of x value and assign ascii value
if sign(x)==-1
    x=abs(x);
    signx=45;           %Assign negative sign
else
    signx=48;           %Assign 0
end

%Test sign of y value and assign ascii value
if sign(y)==-1
    y=abs(y);
    signy=45;
else
    signy=48;
end

```



```

%Scale x and y to gimbal velocity limits (3300)
x=floor(x*3300);
y=floor(y*3300);

%% Input scaling

if sum(buttons(7:9))==0
    ind1=ind1;
else
    %Get index of button pushed
    [val1 ind1]=max(buttons(7:9));
end

switch ind1
    case 1
        ind1=7;
    case 2
        ind1=8;
    case 3
        ind1=9;
end

switch (ind1)
    case 7
        if x < 100
            x = 0;
        end
    case 8
        if x < 100
            x = 0;
        % Scale input to non-linear output for low speed fine tuning
        else if x < 3100
            x = floor(10^(-4)*x^(2.15)); %
        end
    end

        if y < 100
            y = 0;
        else if y < 3100
            y = floor(10^(-4)*y^(2.15));
        end
    end
    case 9
        if x < 100
            x = 0;
        % Scale input to non-linear output for low speed fine tuning
        else if x < 3100
            x = floor(10^(-8.7)*x^(3.49)); %
        end
    end

        if y < 100
            y = 0;
        else if y < 3100
            y = floor(10^(-8.7)*y^(3.49));
        end
    end
end

end

%% Creating gimbal vector
%Convert scaled # to string (each # is a character)
x=num2str(x);
y=num2str(y);
%pause (.25) % for debug

```

```

%Create ASCII vectors from character string
pan=double(x);
tilt=double(y);

%Test vector lengths and add pad zeros if needed
plength=length(pan);
if plength<4
    pzeros=ones(1,4-plength)*48;
    pan=[pzeros pan];
end

tlength=length(tilt);
if tlength<4
    tzeros=ones(1,4-tlength)*48;
    tilt=[tzeros tilt];
end

%Create gimbal command vector to send
gimbalvec=[116 115 signy tilt 10 112 115 signx pan 10];

%% Camera command vector
%Get index of button pushed
[val2 ind2]=max(buttons(1:6));

%Test if any buttons are pushed
if sum(buttons(1:6))~=0
    %Send stop zoom if no button pushed
    cameravec=[129 1 4 7 0 255];
else
    %Which button was pressed
    switch (ind2)
    %Button 1: Zoom In
    case 1
        cameravec=[129 1 4 7 39 255];

    %Button 2: Zoom Out
    case 2
        cameravec=[129 1 4 7 55 255];

    %Button 3: Digital Zoom On
    case 3
        cameravec=[129 1 4 6 2 255];

    %Button 4: IR Filter Off
    case 4
        cameravec=[129 1 4 1 3 255];

    %Button 5: Digital Zoom Off
    case 5
        cameravec=[129 1 4 6 3 255];

    %Button 6: IR Filter On
    case 6
        cameravec=[129 1 4 1 2 255];
    end
end

end

%% Send serial data
%Send commands over serial port
fwrite(com,[gimbalvec cameravec]);

end

%Halt gimbal and halt camera (make sure it is received by sending it
%multiple times) (the 48 after 112 is what the split code is looking for to
%halt the gimbal and terminate the program, the rest is filler for buffer)
fwrite(com,[116 48 48 48 48 48 48 48 48 48 48 48 48 48 48 48 104 10 129 1 4 7 0 255 ])
pause (.25)
fwrite(com,[116 48 48 48 48 48 48 48 48 48 48 48 48 48 48 48 104 10 129 1 4 7 0 255 ])

```

```
pause (.25)
fwrite(com,[116 48 48 48 48 48 48 48 48 48 48 48 48 48 104 10 129 1 4 7 0 255 ])
pause (.25)
fwrite(com,[116 48 48 48 48 48 48 48 48 48 48 48 48 48 104 10 129 1 4 7 0 255 ])
pause off

%Clear output buffer
flushoutput(com);

%Close COM port
fclose(com)

%Close figure
close all
```

## APPENDIX E

### On-board computer split MATLAB code for joystick control

```
%% COM data split code
% Jason Blakely, Mario Czarnomski
% University of North Dakota
%Clear MATLAB workspace
clear all
close all
clc

pause on

%% Set up COM ports

%Get user input for COM port number to use for input data
COMinport=strcat('COM',(num2str(input('Enter COM port number to use for input: '))))

%Get user input for COM port number to use for gimbal output
COMgimbalport=strcat('COM',(num2str(input('Enter COM port number to use for gimbal
output: '))))

%Get user input for COM port number to use for camera output
COMcameraport=strcat('COM',(num2str(input('Enter COM port number to use for camera
output: '))))

%Set up serial COM input port
comin=serial(COMinport,'Baudrate',9600,'Databits',8,'ByteOrder','bigEndian','inputbuffers
ize',44);
fopen(comin);

%Set up serial COM gimbal output port
comgimbal=serial(COMgimbalport,'Baudrate',9600,'Databits',8,'ByteOrder','bigEndian','outp
utbuffersize',16);
fopen(comgimbal);

%Set up serial COM camera output port
comcamera=serial(COMcameraport,'Baudrate',9600,'Databits',8,'ByteOrder','bigEndian','outp
utbuffersize',6);
fopen(comcamera);

%% Gimbal setup
%Change gimbal mode to pure velocity (CV)
fprintf(comgimbal, 'cv');

%Disable command echo from gimbal
fprintf(comgimbal, 'ed');
fprintf(comgimbal, 'ft');

%Set gimbal pan base speed (PB1000)
fprintf(comgimbal, 'pb2000');

%Set gimbal tilt base speed (TB1000)
fprintf(comgimbal, 'tb2000');
```

```

%Set the max tilt velocity (pos/sec)
fprintf(comgimbal, 'tu3300')

%Set the max pan velocity (pos/sec)
fprintf(comgimbal, 'pu3300')

%Set gimbal acceleration to (pos/sec^2)
fprintf(comgimbal, 'pa6000')
fprintf(comgimbal, 'ta6000')

%Allow pan and tilt to operate at higher load using more current
fprintf(comgimbal, 'phr')
fprintf(comgimbal, 'pmh')
fprintf(comgimbal, 'tmh')
fprintf(comgimbal, 'thr')

stop=1;
while (stop~=48)

flushinput(comin);

%Read COM input port
com_in=fread(comin);

%Find T header (116)
n=1;
while com_in(n)~=116;
n=n+1;
end

%16 byte combined command
com_in2=com_in(n:n+21);

%Get gimbal tilt command vector
gimbal_tilt=com_in2(1:8);

%Get gimbal pan command vector
gimbal_pan=com_in2(9:16);

%Get camera command vector
cameravector=com_in2(17:22)

%Send gimbal tilt command
fwrite(comgimbal, gimbal_tilt);
pause (.1)
%Send gimbal pan command
fwrite(comgimbal, gimbal_pan);

%Send camera command
fwrite(comcamera, cameravector);
pause (.05)

stop=gimbal_tilt(2)

end

%Halt Gimbal and Close COM ports
fprintf(comgimbal,'h');
pause (.25)
fwrite(comgimbal, [104 10]);
pause (.25)
fwrite(comgimbal, [104 10]);

pause off
fclose(comin)
fclose(comgimbal)
fclose(comcamera)

```

## APPENDIX F

### The Super Hauler model as it appears in .txt file read by autopilot

```
// Simulator model for the Super Hauler model airplane
// Created By Mario Czarnomski and Richie Spitsberg
// UASE Team 6/5/2008

//----- AERODYNAMICS -----//

// Aerodynamics data from AVL
Alpha_sweep_xml_file=alpha_MNC.xml

// Mapping of the channel numbers in AVL to channel numbers in the Super Hauler
// Right flap
Channel_d1=9
// Right aileron
Channel_d2=5
// Left aileron
Channel_d3=0
// Left flap
Channel_d4=4
// Elevator
Channel_d5=1
// Rudder
Channel_d6=3

// Wing span and area included the space from the fuselage
Wing_Area=2.38
Wing_Span=3.6576
Wing_Taper=1
// Wing incidence
Wing_Incidence=1

// The middle part of the wing is flat ,but it has dihedral on the outer 91Includ.
Wing_Dihedral=2

// We don't know where the cg is, so we assume it has the same x-position as the AC, but it is 7.5 in. below
Wing_X=0.0
Wing_Z=-0.1905

// Tail area and span 91Include the space from the fuselage
Tail_Area=0.5184
Tail_Span=1.092
Tail_Taper=1
Tail_X=-1.8328
```

```

// Fin
Left_Fin_Area=0.045
Left_Fin_Span=0.254
Left_Fin_Taper=0.6
Left_Fin_Parasitic_Drag=0.012
Left_Fin_Span_Efficiency=0.9
Left_Fin_X=-.711
Left_Fin_Z=0.0
Left_Fin_Y=0.0

// Fuselage is 12.75" x 11.5" diameter and 144" long,
// most of it is behind AC, so no destabilizing effect
// Fuselage AC location
Fuse_X=0.0
Fuse_Y=0.0
Fuse_Z=0.0
// X-position of the fuselage nose
Fuse_NoseX=0.9652
// Fuselage length
Fuse_Length=2.5908
// Fuselage max width and height
Fuse_Width=0.32385
Fuse_Height=0.3937
// Fuselage width and height at 1/4 of its length
Fuse_Width1=0.32385
Fuse_Height1=0.34925
// Fuselage width and height at 3/4 of its length
Fuse_Width2=0.1778
Fuse_Height2=0.2286
// Fuselage parasitic drag
Fuse_Parasitic_Drag=0.08

//----- INERTIA -----//

// Now we need the inertia data, let sim calculate pitch,
// roll, and yaw inertia. The gross mass includes 30lb payload and 6.5lb of gas
Gross_Mass=38.33
Empty_Mass=35.38
Wing_Mass=5.35
Fuselage_Mass=12.95
Tail_Mass=.5936
Left_Fin_Mass=.247
Left_Engine_Mass=2.63

//----- PROPULSION -----//

// Engine data for DA-100,9.8hp engine
Left_Engine_Channel=2
Left_Engine_LUT=DA_100.lut

// Propeller data, Vess 27x9.5 inch diameter.
Left_Prop_Diameter=0.6858
// Position of propeller hub wrt to aircraft cg, in m
Left_Prop_X=0.8699
// Moment of inertia in kg/m^2
Left_Prop_Inertia=0.0078
// Propeller coefficients look-up table
Left_Prop_LUT=Vess 27x9.5 Piccolo Final.prd

```

//----- GROUND CONTACT POINTS -----//

ContactPoint\_Top\_Position\_X=0  
ContactPoint\_Top\_Position\_Y=0  
ContactPoint\_Top\_Position\_Z=-0.1905

ContactPoint\_Bottom\_Position\_X=0  
ContactPoint\_Bottom\_Position\_Y=0  
ContactPoint\_Bottom\_Position\_Z=0.1905

ContactPoint\_Nose\_Position\_X=0.9652  
ContactPoint\_Nose\_Position\_Y=0  
ContactPoint\_Nose\_Position\_Z=-0.0381

ContactPoint\_Tail\_Position\_X=-1.93625  
ContactPoint\_Tail\_Position\_Y=0  
ContactPoint\_Tail\_Position\_Z=0.0762

ContactPoint\_Lwing\_Position\_X=0  
ContactPoint\_Lwing\_Position\_Y=-1.8288  
ContactPoint\_Lwing\_Position\_Z=-0.26035

ContactPoint\_Rwing\_Position\_X=0  
ContactPoint\_Rwing\_Position\_Y=1.8288  
ContactPoint\_Rwing\_Position\_Z=-0.26035

ContactPoint\_Lstab\_Position\_X=-1.8415  
ContactPoint\_Lstab\_Position\_Y=-0.5461  
ContactPoint\_Lstab\_Position\_Z=-0.06985

ContactPoint\_Rstab\_Position\_X=-1.8415  
ContactPoint\_Rstab\_Position\_Y=0.5461  
ContactPoint\_Rstab\_Position\_Z=-0.06985

ContactPoint\_Fin\_Position\_X=-1.7907  
ContactPoint\_Fin\_Position\_Y=0  
ContactPoint\_Fin\_Position\_Z=-0.4445

LeftWheel\_Position\_X=-0.1397  
LeftWheel\_Position\_Y=-0.46355  
LeftWheel\_Position\_Z=0.4445

RightWheel\_Position\_X=-0.1397  
RightWheel\_Position\_Y=0.46355  
RightWheel\_Position\_Z=0.4445

NoseWheel\_Position\_X=0.64135  
NoseWheel\_Position\_Y=0  
NoseWheel\_Position\_Z=0.4445  
NoseWheel\_RudderWheelRatio=-1  
NoseWheel\_Steering\_Channel=8

//----- AVIONICS MOUNTING -----//

// Avionics (IMU sensor) orientation with respect to the aircraft body axes  
// Euler angles in deg  
IMU\_Sensor\_Roll\_Angle=0.0  
IMU\_Sensor\_Pitch\_Angle=0.0



```
IMU_Sensor_Yaw_Angle=0.0
```

```
// Avionics (IMU sensor) position vector with respect to the aircraft CG, in body axes
```

```
// Vector components in m
```

```
IMU_Sensor_Position_X=-0.53975
```

```
IMU_Sensor_Position_Y=0.0
```

```
IMU_Sensor_Position_Z=-0.00635
```

## APPENDIX G

### Controller gains settings in Piccolo Command Center

**Controller Configuration - Piccolo '1474'**

Lat Gains | Lon Gains | Trims | Limits | Vehicle | Mixing | Landing | Launch | Sensor Navigation

Open... | Save... | Request All | Send All | Set to Defaults

Section	Parameter	Value	Units
Tangent Orbit Tracking	OnOff	0	
	Roll err to roll rate cmd	1.000	
	Roll rate lpf cutoff	10.00	[Hz]
	Roll rate err to aileron	0.0000	
	Roll rate err int to aileron	0.7500	
Yaw control	Lat accel err int to roll	0.0000	
	Yaw rate lpf cutoff	10.00	[Hz]
	Yaw rate err to rudder	1.0000	
Manual yaw control	Side force err int to rudder	0.0000	
	Manual yaw rate to rudder	0.0000	
Steering control	Y to Vy scaling power	0.0000	
	Track Y to Vy	0.2000	
	Track Vy err int to nose gear	0.0500	
	Track Vy err pro to nose gear	0.2000	
	Yaw rate to nose gear	0.0000	
	Vy to nosegear scaling power	1.0000	
Track control	Tracker convergence	0.2500	
	Heading err to turn rate	0.5500	
	Heading err der to turn rate	0.2000	
	Turn err lpf cutoff	0.00	[Hz]

**Controller Configuration - Piccolo '1474'**

Lat Gains | Lon Gains | **Trims** | Limits | Vehicle | Mixing | Landing | Launch | Sensor Navigation

Open... | Save... | Request All | Send All | Set to Defaults

<b>Total energy control</b> Alt err to alt rate: 0.200 Throttle lpf cutoff: 0.00 [Hz] Throttle Prediction Trust: 0.0000 Energy rate err int to throttle: 1.0000 Energy rate err int to flap: 0.0000		<b>Pitch damper</b> Pitch rate lpf cutoff: 5.00 [Hz] Pitch err to elevator: 0.0000 Pitch rate err to elevator: 0.0000	
<b>Z Acceleration control</b> Elevator Prediction Trust: 0.75 Acceleration lpf cutoff: 5.00 [Hz] Accel err to elevator: 0.0000 Accel err int to elevator: 1.5000 Accel cmd lpf cutoff: 0.00 [Hz]		<b>RPM control</b> RPM err to RPM rate cmd: 2.50 RPM rate err int to throttle: 0.000200	
<b>Airspeed control</b> TAS err to TAS rate: 0.15 TAS rate err to accel cmd: 1.0000		<b>Brakes control</b> Accel err int to brakes: 1.00	
<b>Altitude control</b> Slow IAS error threshold: 194.38 [kts] Fast IAS error threshold: 8.75 [kts]			

**Controller Configuration - Piccolo '1474'**

Lat Gains | Lon Gains | **Trims** | Limits | Vehicle | Mixing | Landing | Launch | Sensor Navigation

Open... | Save... | Request All | Send All | Set to Defaults

<b>Trims</b> Aileron: 2.00 [deg] Elevator: 1.93 [deg] Throttle: 0.50 Rudder: -1.00 [deg] Flap: 0.00 [deg] Nosegear: 0.00 [deg]	
--	--



Controller Configuration - Piccolo '1474'

Lat Gains | Lon Gains | Trims | Limits | Vehicle | **Mixing** | Landing | Launch | Sensor Navigation

Open... | Save... | Request All | Send All | Set to Defaults

Mixing

Throttle to rudder	0.00	[deg]
Flap to elevator	0.10	
Aileron to rudder	0.00	
Aileron differential	0.00	
Flaperon ratio	0.00	
Manual Rudder to nose gear	1.00	
Auto Nose gear to rudder	0.80	
Rudder differential	0.00	

Controller Configuration - Piccolo '1474'

Lat Gains | Lon Gains | Trims | Limits | Vehicle | Mixing | **Landing** | Launch | Sensor Navigation

Open... | Save... | Request All | Send All | Set to Defaults

Landing Type

Type: Wheeled

Pattern

Approach Slope	4.00	[deg]
Short Final Slope	4.00	[deg]
Pattern Max AGL	0.000	[ft]
Approach time	40.00	[s]
Go around time	20.00	[s]
Cross time	20.00	[s]

Configuration

Flap setting	0.00	[deg]
Approach Speed fraction	1.10	
Short Final Speed fraction	1.10	
Touchdown Speed fraction	-1.00	

Decision

Y max error	15.00	[ft]
Z max error	6.56	[ft]
Max overspeed	5.83	[kts]

Flare

Engine kill time	-1.00	[s]
Sink rate	-1.944	[kts]
Flare height	2.016	[ft]

Rollout

Rolling elevator	0.00	[deg]
Deceleration cmd	1.50	[m/s/s]
Rollout wing leveling	0	

Controller Configuration - Piccolo '1474'

Lat Gains | Lon Gains | Trims | Limits | Vehicle | Mixing | Landing | Launch | Sensor Navigation

Open... | Save... | Request All | Send All | Set to Defaults

<p>Launch Type</p> <p>Type: <input type="text" value="Wheeled"/></p>	<p>Speeds and time</p> <p>Throttle hold time: <input type="text" value="5.00"/> [s]</p> <p>Climb speed fraction: <input type="text" value="1.10"/></p> <p>Climbout time: <input type="text" value="10.00"/> [s]</p>
<p>Prelaunch</p> <p>Flaps: <input type="text" value="0.00"/> [deg]</p> <p>Throttle: <input type="text" value="0.50"/></p> <p>Brakes: <input type="text" value="0.00"/></p>	<p>Action times</p> <p>Action 1 time: <input type="text" value="0.00"/> [s]</p> <p>Action 2 time: <input type="text" value="0.00"/> [s]</p> <p>Action 3 time: <input type="text" value="0.00"/> [s]</p>
<p>Safety checks</p> <p>Max cross error: <input type="text" value="16.4"/> [ft]</p> <p>Minimum RPM: <input type="text" value="0"/></p>	
<p>Engine control</p> <p>Acceleration: <input type="text" value="4.00"/> [m/s/s]</p> <p>Slow Throttle rate: <input type="text" value="0.040"/> [s]</p> <p>Fast Throttle rate: <input type="text" value="0.100"/> [s]</p> <p>Throttle switch speed: <input type="text" value="5.83"/> [kts]</p>	
<p>Rotation</p> <p>Rolling elevator: <input type="text" value="0.00"/> [deg]</p> <p>Rotation elevator: <input type="text" value="-10.00"/> [deg]</p> <p>Rotation time: <input type="text" value="0.50"/> [s]</p>	

## REFERENCES

- [1] Gerhard A. Koepf, Robert G. Marshalek, and David L. Begley, "Space Laser Communications: A Review of Major Programs in the United States," in *AEU-International Journal of Electronics and Communications*, Volume 56, Issue 4, 2002, Pages 232-242.
- [2] Karl Meinzer, Dante Bauer, Dick Jansson, Hermann Günther, "Infrared Laser on P3-D," *AMSAT-dl Journal*, 1/2000.
- [3] D. Russell, H. Ansari, C.-C. Chen, "Lasercom pointing, acquisition and tracking control using a CCD-based tracker," in *Free-Space Laser Communication Technologies VI*, G. Stephen Mecherle, Editor, Proceedings of the SPIE Vol. 2123, pp. 294-303 (1994).
- [4] Gerardo G. Ortiz, Shinhak Lee, Steve Monacos, Malcolm Wright and Abhijit Biswas, "Design and Development of a Robust ATP Subsystem for the Altair UAV-to-Ground Lasercomm 2.5 Gbps Demonstration," in *Free-Space Laser Communication Technologies XV*, G. Stephen Mecherle, Editor, Proceedings of the SPIE Vol. 4975, pp. TBD (2003).
- [5] W. Farr, B. Liu and S. P. Monacos, "Characterization of the random-access-windowing CCD camera for optical comm ATP Subsystem," in *Free-Space Laser Communication Technologies XV*, G. Stephen Mecherle, Editor, Proceedings of the SPIE Vol. 4975, pp. TBD (2003).
- [6] Abhijit Biswas, Joseph Kovalik, Martin W. Regehr, Malcolm Wright, "Emulating an Optical Planetary Access Link with an Aircraft," in *Free-Space Laser Communication Technologies XXII*, Hamid Hemmati, Editor, Proceedings of the SPIE Vol. 7587, 75870B, (2010).
- [7] Industrial Fiber Optics, "Diode Lab Lasers Data Sheet," available on the World Wide Web at <<http://i-fiberoptics.com/lasers.php?cat=diode-lab-lasers>>. Accessed on June, 2010.
- [8] Industrial Fiber Optics, "Video Laser Modules Operator's Manual," available on the World Wide Web at <<http://i-fiberoptics.com/pdf/120235-RevE.pdf>>. Accessed on June, 2010.

- [9] Pacific Silicon Sensor Incorporated, "Pacific Silicon Sensor Solderable Series Data Sheet," available on the World Wide Web at <[http://www.pacific-sensor.com/pdf\\_solderable/PS95-F-CH.pdf](http://www.pacific-sensor.com/pdf_solderable/PS95-F-CH.pdf)>. Accessed on June 2010.
- [10] Blue Sky Research, "VPSL-Virtual Point Source Laser," available on the World Wide Web at <<http://www.blueskyresearch.com/c/b/posts/view/37>>. Accessed on June 2010.
- [11] Dragon Lasers, "Laser Beam Expander," available on the World Wide Web at <<http://www.dragonlasers.com/product.php?productid=16332&cat=285&page=1>>. Accessed on June 2010.
- [12] Pacific Silicon Sensor Incorporated, "Solderable Photodiodes," available on the World Wide Web at <[http://www.pacific-sensor.com/pages/sp\\_solderable.html](http://www.pacific-sensor.com/pages/sp_solderable.html)>. Accessed on June 2010.
- [13] SpectroFilm, "Laser Diode Filters," available on the World Wide Web at <<http://spectrofilm.com/laserdiode.htm>>. Accessed on June 2010.
- [14] Advanced Digital Logic, "New Family of Embedded PC," available on the World Wide Web at <<http://www.adl-usa.com/index.php>>. Accessed on June 2010.
- [15] Advanced Digital Logic, "ADL945PC Specifications," available on the World Wide Web at <<http://www.adl-usa.com/products/cpu/datapage.php?pid=ADL945PC>>. Accessed on June 2010.
- [16] Advanced Digital Logic, "Embedded PC104 Power Supplies," available on the World Wide Web at <<http://www.adl-usa.com/products/powersupplies/datapage.php?pid=HPS3512>>. Accessed on June 2010.
- [17] Versa Logic Corporation, "VL-ENCL-4 Ruggedized Enclosure," available on the World Wide Web at <<http://versalogic.com/products/ds.asp?productid=114>>. Accessed on June 2010.
- [18] Advanced Digital Logic, "PC/104-Plus Peripherals," available on the World Wide Web at <<http://www.adl-usa.com/products/peripherals/datapage.php?pid=MSMX104%2B>>. Accessed on June 2010.
- [19] Directed Perception FLIR Motion Control Systems, "PTU-D46-17P70T Model," available on the World Wide Web at <<http://www.dperception.com/products/ptu-d46/ptu-d46-17p70t/>>. Accessed on June 2010.



- [20] Directed Perception FLIR Motion Control Systems, "Model PTU-D46-17P70T Quick Configuration Guide," available on the World Wide Web at <<http://www.dperception.com/pdf/PTU-D46-Config.pdf>>. Accessed on June 2010.
- [21] Mariusz Czarnomski, Jason Blakely, Ziming Wang, Gregory Williamson, Richard R. Schultz, and William H. Semke, "Laser Communications for Unmanned Aircraft Systems Using Differential GPS IMU Data," in Free-Space Laser Communication Technologies XXII, Hamid Hemmati, Editor, Proceedings of the SPIE Vol. 7587, 758709, (2010).
- [22] Buskier, M., "Statistically Significant Factors that Affect Pointing Accuracy of Airborne Remote Sensing Payload," Master's Thesis, Department of Mechanical Engineering, University of North Dakota, 2007.
- [23] Cloud Cap Technology, "Communications for the Piccolo avionics," available on the World Wide Web at <[http://www.cloudcaptech.com/piccolo\\_system.shtm#flight](http://www.cloudcaptech.com/piccolo_system.shtm#flight)>. Accessed on June 2010.
- [24] Directed Perception, "Computer Controlled Pan-Tilt Unit Model PTU-D46 User Manual," available on the World Wide Web at <<http://www.dperception.com/pdf/products/PTU-D46/PTU-manual-d46.pdf>>. Accessed on June 2010.
- [25] Nitin J. Soni, "Integration and Test of High Speed Transmitter Electronics for Free-Space Laser Communications," Proceedings of the 15<sup>th</sup> International Communications Satellite Systems Conference sponsored by AIAA, San Diego, California, February, 1994.